HIGHLY STRETCHABLE ELECTROLUMINESCENT SKIN FOR OPTICAL SIGNALING AND TACTILE SENSING

A Thesis

Presented to the Faculty of the Graduate School

of Cornell University

In Partial Fulfillment of the Requirements for the Degree of

Master of Science

by

SHUO LI

August 2016

ABSTRACT

Biological systems employ a host of strategies for display and camouflage. Cephalopods such as octopuses and cuttlefish have a stretchable skin that allows them to sense external environments and dynamically tune their colors for communication and disguise. Inspired by nature, this work presents a highly stretchable electroluminescent actuator based on intrinsically soft materials such as elastomeric silicone rubbers and transparent ionically conducive hydrogels in a multilayer configuration. This device is capable to accommodate large and various kinds of deformations while actively emitting light. The laminated structure also enables capacitive sensing for touch, pressure, and strains. It can be further monolithically integrated onto a soft robot as an electroluminescent skin, providing it with dynamic coloration and sensory feedback from both external and internal stimuli.

BIOGRAPHICAL SKETCH

Shuo Li was born in Xi'an, China on February 12th, 1992 and he moved to Beijing at the age of ten with his family. After graduating from high school, he went to the United States to pursue his undergraduate degree at University of Illinois, Urbana-Champaign and graduated cum laude in 2014 with a Bachelor of Science in Materials Science & Engineering and a minor in Chemistry. He then came to Cornell University for graduate education, seeking a Master of Science in MSE.

During his time at Illinois, Shuo gained a strong foundation in MSE and a solid understanding of polymer and electronic materials. He also cultivated a keen interest in research with an emphasis on bio-integrated flexible/stretchable electronics since sophomore year, when he joined Professor John Rogers' group as an undergraduate researcher. He was immerged into projects on epidermal electronics and optofluidic drug delivery devices and co-authored three papers in *Advanced Materials*, *Cell*, and *Nature Protocols*.

At Cornell, he extended his research on stretchable electronics and explored its application on soft machines under the advisement of Professor Robert Shepherd. Shuo has used his knowledge of active soft materials to develop a hyper-elastic light-emitting actuator with potential applications in wearables and bio-inspired robotics. This work was published in *Science* and he named a co-first author. He also holds a US provisional patent and has two more journal articles in preparation on related topics.

Shuo will continue his graduate education pursuing a Ph.D. in MSE at Cornell in Professor Shepherd's group starting August 2016.

THIS THESIS IS DEDICATED

TO MY GRANDPA,

THE BRAVEST PERSON I KNOW.

ACKNOWLEDGMENTS

I would like to thank my parents for their continuous support, both mentally and financially, throughout my career as a student. Thanks to my father for sharing with me the valuable experience of doing scientific research and thanks to my mother for providing me the constant encouragement when I was thrilled or depressed. I could not have arrived at this step without you.

I would like to thank my advisor, Professor Robert Shepherd, for his guidance and mentorship during the last two years. He was always a reliable source of innovative ideas and a role model of conducting research. I sincerely appreciate the confidence he gave me to explore possibilities, as well as the enthusiasm he showed for my projects.

I am also grateful to all of the members in our group (Chris, Bryan, Huichan, Ben, Sanlin, Ilse, TJ, Kevin, James, and Wanying) for making these two years in the group a truly enjoyable journey. Thanks especially to Chris and Bryan for the productive collaborations on stretchable displays, and to Huichan for all the academic and entertainment conversations in our native language.

Outside of the group, I would like to acknowledge our collaborators, Dr. Massimo Totaro, Dr. Lucia Beccai, and Dr. Barbara Mazzolai at Italian Institute of Technology for their kind host during my visit to Pontedera and their contribution and discussion on the Science paper.

Finally I would like to extend my gratitude to Professor John Rogers and Professor Peter Bocko for writing me letters of recommendation for my Ph.D. applications despite their busy schedule. I express my sincere thanks to them.

TABLE OF CONTENTS

LIST OF FIGURES

LIST OF TABLES

CHAPTER 1

INTRODUCTION AND THESIS SUMMARY

Introduction

Stretchable Displays

When the commercial implementations of flexible displays that can be rolled up like paper are already available, people start to imagine rubber-like displays that can stretch over large areas or deform to wrap around an object (1). Recent advances in stretchable electronics have introduced appealing applications such as biological health monitoring sensors (2-4), photodetectors on curvilinear geometries (5), and stretchable power sources (6-8). There are two common methods to yield elasticity in material systems for stretchable electronics: (i) mechanically structuring existing, inextensible materials (e.g. silicon) and (ii) designing novel intrinsically conductive materials or composites. The former case typically involves patterning thin films of semiconductors into wavy serpentine or buckled shapes and bonding on an elastomeric substrate (9, 10). The latter choice has been demonstrated by dispersing or printing conductors in an intrinsically elastic matrix (11, 12).

Based on these well-characterized strategies, stretchable displays, an emerging subclass of stretchable electronics, has also witnessed some progress in research works during the recent years. In 2009, Someya and coworkers introduced a stretchable active-matrix organic light-emitting diode (OLED) display based on printable elastic conductors (13). The authors dispersed single-walled carbon nanotubes (SWNTs) in a fluorinated rubber as conductive ink and printed on silicone elastomer to form elastic electrodes. They later combined this electrode with organic transistors and OLED and produced a 16-by-16 grid of display capable to stretch by 30-50% (Fig. 1A). In 2010, Rogers *et al*. presented an ultrathin inorganic light-emitting diodes (ILED) and photodetectors (PD) configured in a noncoplanar serpentine layouts and bonded on a thin, pre-strained sheet of poly(dimethylsiloxane) (PDMS) (14). Their fabricated device is able to accommodate strains up to 75% with other extreme modes of deformation while operating robustly (Fig. 1B). In 2011, Pei and colleagues reported a first demonstration of an intrinsically stretchable polymer light-emitting device (PLED) that also adopts SWNTs-polymer composite electrodes (15). They used a roll lamination process to

fabricate the blue luminescent polymer layer comprising a polyfluorene copolymer, an ionic conductor, and a salt. Although their device provides an alternative path compared to the previously mentioned discrete displays, the elasticity under tensile strain ("stretchability"; about 45% at 70°C) is somehow confined by their substrate material (PtBA), which is a shape memory polymer with a glass transition temperature about 56°C (Fig. 1C).

More recently, Carmichael *et al*. developed a stretchable light-emitting electrochemical cell (LEEC) that uses an ionic transition metal complex (Ru/PDMS) sandwiched between a pair of metallic electrodes (anode: Au/PDMS; cathode: EGaIn liquid metal) to enable elasticity with linear strain up to 27% at room temperature (16) (Fig. 1D). Pei *et al*. has gone one step further and introduced another elastomeric polymer light-emitting device (EPLED) featuring an electroluminescent polymer layer sandwiched between a pair of transparent composite electrodes comprising thin percolation network of silver nanowires (AgNWs) (17). Their fabricated device can emit light when exposed to strains as large as 120% (Fig. 1E).

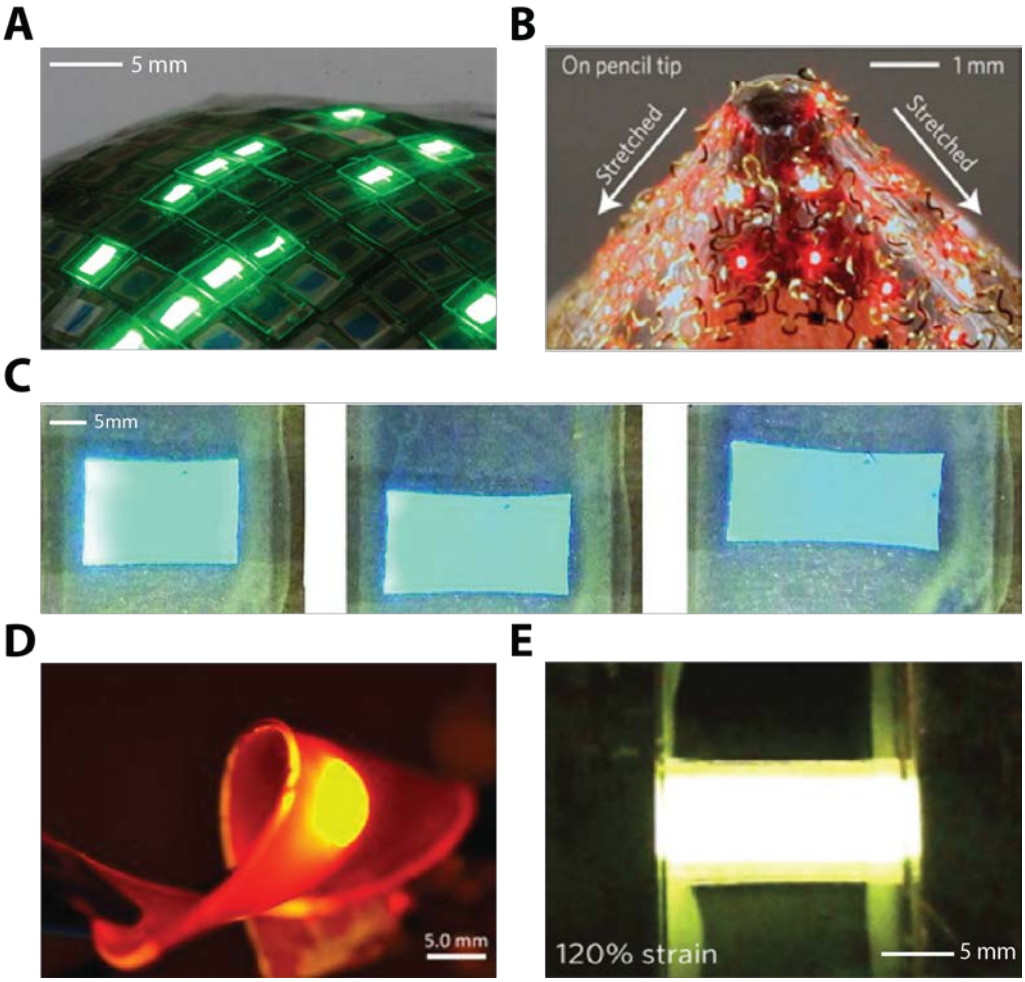

Figure 1. (A) Photograph of a 16-by-16 grid of stretchable active-matrix organic LED spread over a curved surface (13). (B) Photograph of a 6-by-6 array of micro ILEDs tightly stretched and conformed to the tip of a pencil (14). (C) Photographs of a PLED glowing while being stretched under different strains (0%, 20%, and 45%) (15). (D) Photograph of a twisted LEEC (16). (E) Photograph of an EPLED biased at 14V at 120% strain (17).

All of the above examples have been good proof-of-concepts of stretchable displays using different approaches. None of the devices, however, provides adequate stretchability in either uniaxial or biaxial manners, which is critical for new applications including medical imaging, robotics, and large-area displays.

Bioinspired Soft Robots and Colorations

Bioinspiration, adopting phenomena found in biology to stimulate studies in non-living systems, leads to abundant research topics that allow us to appreciate the optimization of functions possessed by nature (18). The goal of this subject is to mimic or imitate the functions or properties of biological systems, rather than understanding or reproducing the complex and fundamental mechanisms behind them. For example, we do not need to fully understand how an octopus controls its tentacles in order to replicate some of its motions and use it as a gripper.

Many advances related to bioinspiration in materials science focus on soft matters: materials that are elastic and easily deformed (19), since softness and body compliance compose the majority of biological systems. Soft robotics, machines made of soft – often-elastomeric – materials (20), provide unique features in the context of both bioinspired designs and robotics, offering limitless opportunities to bridge the gap between machines and people. Figure 2 shows a variety of soft robotics with different modalities and functionalities.

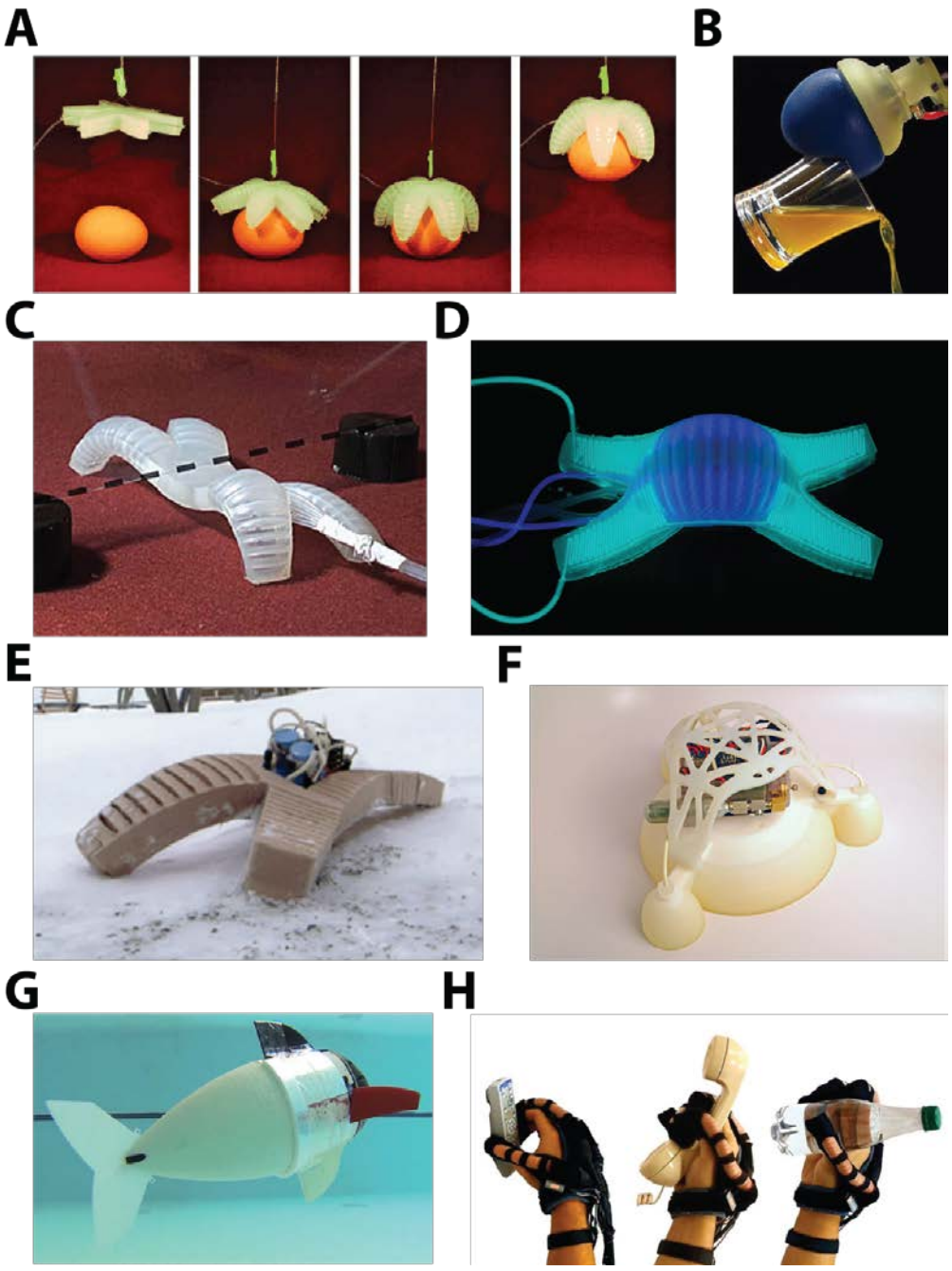

Figure 2. (A) A starfish inspired soft gripper with dexterous grasping (20). (B) A universal gripper based on jamming of granular materials (21). (C) A multi-gait quadruped that can crawl through an obstacle (22). (D) A quadruped using microfluidic for active camouflage (23). (E) A fully untethered soft robot that is resilient to adverse environments (24). (F) A soft robot integrated with 3-D printed hard components powered by combustion (25). (G) An autonomous soft robotics fish for swimming (26). (H) A soft glove for hand rehabilitation (27).

Compared to hard-bodied robots, soft ones have their unique advantages in the following aspects: (i) since they are made out of intrinsically soft materials, such as silicone elastomers or polyurethanes, they can generate continuous deformation with natural locomotion and infinite passive degrees of freedom (28). (ii) The compliant bodies also endow soft robots with remarkable adaptability, allowing them to bend or twist with high curvatures and conform to arbitrary geometries (29). (iii) Also, soft robots are low-cost to build thanks to the liquid phase processing enabled rapid prototyping and manufacturing. (iv) Last, employing materials with elastic modulus similar to that of human skin and tissues given soft robots promise to be biocompatible and bio-integratable (29).

The fabrication methods developed for soft robotics (in particular, pneumatically actuated ones) – soft lithography – are migrated from microfluidics, another area with strong basis in bioinspiration with minor modifications (18) (30). PDMS with networks of air microchannels (pneu-nets) are created by replica molding on 3D printed molds and bonded to another thin slab of PDMS (20). To regulate the deformation, strain-limiting

materials (i.e. a stiffer rubber or inextensible fibers) were incorporated so that inflation would result in continuous yet limited motions (Fig. 2 A, C, D, and E).

Biology also provides us with numerous examples of natural actuators. For instance, the ability for a cephalopod to sense its surroundings and modulate its skin color (for visual display and camouflage) remains an inspiration for the biologists and engineers (31). In the fields of chemistry, materials science, and microelectronics, people have shown intense interests to imitate and reproduce this feature.

In 2012, Whitesides *et al*. presented a soft machine integrated with microfluidic networks offering both display/camouflage and locomotion (23). Pumping liquid dyes or pigments into the overlaid microfluidic channels can actively change color, luminescence, and pattern of the soft machines. Meanwhile, additional microchannels embedded in highly extensible elastomers provide the pneumatic actuation for walking (Fig. 3A). In 2014, Zhao and colleagues introduced a soft materials system named electro-mechano-chemically responsive (EMCR) elastomer as synthetic chromatophores (pigment-containing sacs under cephalopods' skin) to induce various on-demand

fluorescent patterns (32). The versatile coloration enabled by stretching the mechanochromic molecules embedded in a stretchable elastomer provides a novel and straightforward path to mimic the activation of chromatophores. In addition, a pattern of wrinkles happens in response to an applied electric field, which creates reversible deformations and subsequently yields on-demand fluorescent patterns (Fig. 3B). Also in 2014, Rogers and coworkers invented an adaptive optoelectronic camouflage sheet comprising photodiodes, thermosensitive polymer, and reflective background (33). An incident beam of light on the system stimulates the photodetectors and thus activates the local joule heaters embedded underneath, which would fade the thermosensitive polymer and expose the reflective background (Fig. 3C). This device is capable of generating distributed, multipixeled black-and-white patterns that spontaneously and rapidly match the ambient environment for communication and camouflage purposes.

Given all these great engineering efforts, it is still challenging to replicate all the functions that cephalopod skins possess; for example, the agility of color switch, the richness of colors, and the sensory feedbacks, which remain inspiration for future works.

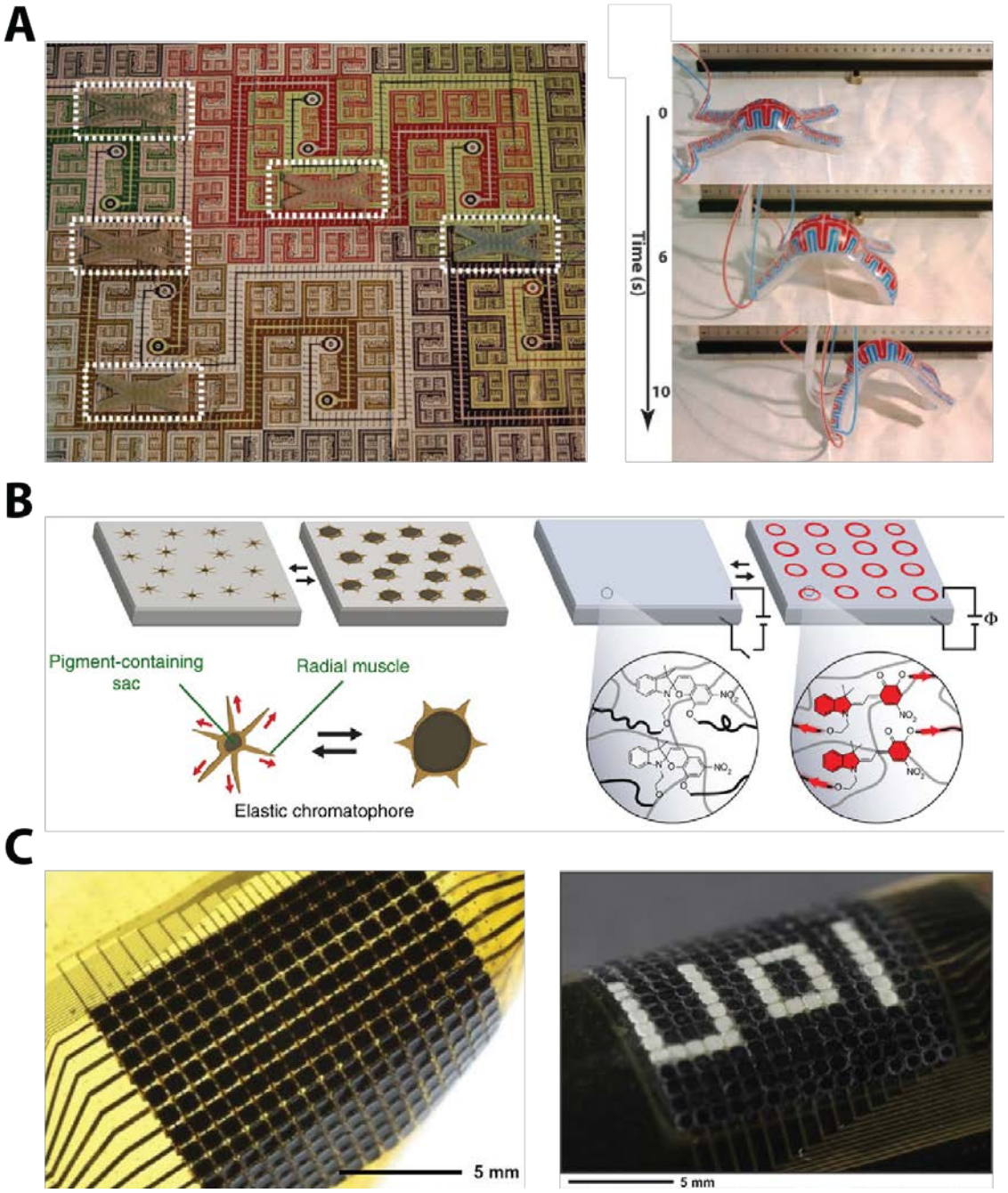

Figure 3. (A) Camouflage of soft robots in an artificial environment with five of them seating in different locations and adopting the coloration for background matching (left); a color layer integrated soft quadruped undulate to walk (23). (B) Schematic of the coloration controlled by stretching/releasing (left) and on-demand fluorescent pattern change controlled by applied voltage (right) (32). (C) Photograph of a bent multipixeled device (left) and a device operating while bent, showing the text “U o I” with adaptive pattern matching (right) (33).

Thesis Summary

In this thesis, the design, fabrication, and applications of a highly stretchable light-emitting actuator are described. Inspired by the skins of some cephalopods, an alternative method based on soft lithography is adopted to generate stretchable displays with intrinsically compliant materials (silicone elastomers, hydrogels, etc.). This fabricated device is then integrated onto a crawling soft robot to demonstrate its capability of accommodating large uniaxial or areal deformations with capacitive tactile sensing.

This thesis is organized into three chapters. After the introduction that illustrates the background and motivation of this research, Chapter 2 presents the main text of the paper published in Science (Larson *et al.*, *Science* 351, 1071-1074, 2016). Chapter 3 is the supplementary materials of the paper that contain methods and materials in details as well as additional experimental setups and results.

REFERENCE

1. M. C. LeMieux, Z. Bao, Flexible electronics: Stretching our imagination. *Nat. Nanotech.* **327**, 585-586 (2008).
2. D.-H. Kim, N. Lu, R. Ma, Y.-S. Kim, R.-H. Kim, S. Wang, J. Wu, S.M. Won, H. Tao, A. Islam, K.J. Yu, T.-I. Kim, R. Chowdhury, M. Ying, L. Xu, M. Li, H.-J. Chung, H. Keum, M. McCormick, P. Liu, Y.-W. Zhang, F.G. Omenetto, Y. Huang, T. Coleman and J.A. Rogers, Epidermal electronics. *Science* **333**, 838-843 (2011).
3. J.-W. Jeong, W.-H. Yeo, A. Akhtar, J.J.S. Norton, Y.-J. Kwack, S. Li, S.-Y. Jung, Y. Su, W. Lee, J. Xia, H. Cheng, Y. Huang, W.-S. Choi, T. Bretl and J.A. Rogers, Materials and optimized designs for human-machine interfaces via epidermal electronics. *Adv. Mater.* **25**, 6839-6846 (2013).
4. R.C. Webb, A.P. Bonifas, A. Behnaz, Y. Zhang, K.J. Yu, H. Cheng, M. Shi, Z. Bian, Z. Liu, Y.S. Kim,W.-H. Yeo, J.S. Park, J. Song, Y. Li, Y. Huang, A.M. Gorbach and J.A. Rogers, Ultrathin conformal devices for precise and continuous thermal characterization of human skin. *Nat. Mater.* **12**, 938-944 (2013).
5. H. C. Ko, M. P. Stoykovich, J. Song, V. Malyarchuk, W. M. Choi, C.-J. Yu, J. B. Geddes, J. Xiao, S. Wang, Y. Huang and J. A. Rogers, A hemispherical electronic eye camera based on compressible silicone optoelectronics. *Nature* **454**, 748-753 (2008).
6. D. J. Lipomi, B. C.-K. Tee, M. Vosgueritchian, Z. Bao, Stretchable organic solar

cells. *Adv. Mater*. **23**, 1771-1775 (2011).

7. S. Xu, Y. Zhang, L. Jia, K.E. Mathewson, K.-I. Jang, J. Kim, H. Fu, X. Huang, P. Chava, R. Wang, S. Bhole, L. Wang, Y.J. Na, Y. Guan, M. Flavin, Z. Han, Y. Huang, J.A. Rogers, Soft microfluidic assemblies of sensors, circuits, and radios for the skin. *Science* **344**, 70-74 (2014).
8. Z. Song, X. Wang, C. Lv, Y. An, M. Liang, T. Ma, D. He, Y.-J. Zheng, S.-Q. Huang, H. Yu, H. Jiang, Kirigami-based stretchable lithium-ion batteries. *Sci. Rep.* **5**, 10988 (2015).
9. D.-H. Kim, J.-H. Ahn, W. M. Choi, H.-S. Kim, T.-H. Kim, J. Song, Y. Huang, Z. Liu, C. Lu, J. A. Rogers, Stretchable and foldable integrated circuits. *Science* **320**, 507-511 (2008)
10. D.-H. Kim, J. Song, W. M. Choi, H.-S. Kim, R.-H. Kim, Z. Liu, Y. Huang, K.-C. Hwang, Y.-W. Zhang, J. A. Rogers, Materials and noncoplanar mesh designs for integrated circuits with linear elastic responses to extreme mechanical deformations. *Proc. Natl. Acad. Sci. U.S.A.* **105**, 18675-18680 (2008).
11. T. Sekitani, H. Nakajima, H. Maeda, T. Fukushima, T. Aida, K. Hata, T. Someya, A rubberlike stretchable active matrix using elastic conductors. *Science* **321**, 1468-1472 (2008).
12. M. Kujawski, J. D. Pearse, F. Smela, Elastomer filled with exfoliated graphite as compliant electrodes. *Carbon* **48**, 2409-2417 (2010).

13. T. Sekitani, H. Nakajima, K. Maeda, T. Fukushima, T. Aida, K. Hata, T. Someya, Stretchable active-matrix organic light-emitting diode display using printable elastic conductors. *Nat. Mater.* **8**, 494-499 (2009).

14. R.-H. Kim, D.-H. Kim, J. Xiao, B.H. Kim, S.-I. Park, B. Panilaitis, R. Ghaffari, J. Yao, M. Li, Z. Liu, V. Malyarchuk, D.G. Kim, A.-P. Le, R.G. Nuzzo, D.L. Kaplan, F.G. Omenetto, Y. Huang, Z. Kang and J.A. Rogers, Waterproof AlInGaP optoelectronics on stretchable substrates with applications in biomedicine and robotics. *Nat. Mater.* **9**, 929-937 (2010).

15. Z. Yu, X. Niu, Z. Liu, Q. Pei, Intrinsically stretchable polymer light-emitting devices using carbon nanotube-polymer composite electrodes. *Adv. Mater.* **23**, 3989-3994 (2011).

16. H. L. Filiatrault, G. C. Porteous, R. S. Carmichael, G. J. E. Davidson, T. B. Carmichael, Stretchable light-emitting electrochemical cells using an elastomeric emissive material. *Adv. Mater.* **4**, 2673-2678 (2012).

17. J. Liang, L. Li, X. Niu, Z. Yu, Q. Pei, Elastomeric polymer light-emitting devices and displays. *Nat. Photonics.* **7**, 817-824 (2013).

18. G. M. Whitesides, Bioinspiration: something for everyone. *Interface Focus* **5**, 20150031 (2015).

19. I. W. Hamley, *Introduction to soft matter: synthetic and biological self-assembling materials*. (John Wiley & Sons, UK, 2013).

20. F. Ilievski, A. D. Mazzeo, R. F. Shepherd, X. Chen, G. M. Whitesides, Soft robotics for chemists. *Angew. Chem. Int. Ed.* **50**, 1890-1895 (2011).

21. E. Brown, N. Rodenberg, J. Amend, A. Mozeika, E. Steltz, M. R. Zakin, H. Lipson, H. M. Jaeger, Universal robotic gripper based on the jamming of granular material. *Proc. Natl. Acad. Sci. U.S.A.* **107**, 18809-18814 (2010).

22. R. F. Shepherd, F. Ilievski, W. Choi, S. A. Morin, A. A. Stokes, A. D. Mazzeo, X. Chen, M. Wang, G. M. Whitesides, Multigait soft robot. *Proc. Natl. Acad. Sci. U.S.A.* **108**, 20400-20403 (2012).

23. S. A. Morin, R. F. Shepherd, S. W. Kwok, A. A. Stokes, A. Nemiroski, G. M. Whitesides, Camouflage and display for soft machines. *Science* **337**, 828-832 (2012).

24. M. T. Tolley, R. F. Shepherd, B. Mosadegh, K. C. Galloway, M. Wehner, M. Karpelson, R. J. Wood, G. M. Whitesides, A resilient, untethered soft robot. *Soft Robotics* **1**, 213-223 (2014).

25. N. W. Barlett, M. T. Tolley, J. T. B. Overvelde, J. C. Weaver, B. Mosadegh, K. Bertoldi, G. M. Whitesdies, R. J. Wood, A 3D-printed, functionally graded soft robot powered by combustion. *Science* **349**, 161-165 (2015).

26. R. K. Katzschmann, A. D. Marchese, D. Rus, Hydraulic autonomous soft robotic fish for 3D swimming. *Proc. International Symposium on Experimental Robotics*, 1122374 (2014).

27. P. Polygerinos, Z. Wang, K. C. Galloway, R. J. Wood, C. J. Walsh, Soft robotic glove for combined assistance and at-home rehabilitation. *Robot. Auton. Syst.* **73**, 135-143 (2015).

28. F. Saunders, E. Golden, R. D. White, J. Rife, Experimental verification of soft-robot gaits evolved using a lumped dynamic model. *Robotica* **29**, 823-830 (2011).

29. D. Rus, M. T. Tolley, Design, fabrication and control of soft robots. *Nature* **521**, 467-475 (2015).

30. Y. Xia, G. M. Whitesides, Soft lithography. *Annu. Rev. Mater. Sci.* **37**, 551-575 (1998).

31. R. T. Hanlon, Cephalopod dynamic camouflage. *Curr. Biol.* **17**, R400-R404 (2007).

32. Q. Wang, G. R. Gossweiler, S. L. Craig, X. Zhao, Cephalopod-inspired design of electro-mechano-chemically responsive elastomers for on-demand fluorescent patterning. *Nat. Commun.* **5**, 4899 (2014).

33. C. Yu, Y. Li, X. Zhang, V. Malyarchuk, S. Wang, Y. Shi, L. Gao, Y. Su, Y. Zhang, H. Xu, R. T. Hanon, Y. Huang, J. A. Rogers, Adaptive optoelectronic camouflage systems with designs inspired by cephalopod skins. *Proc. Natl. Acad. Sci. U.S.A.* **111**, 12998-13003 (2014).

CHAPTER 2

HIGHLY STRETCHABLE ELECTROLUMIENSCENT SKIN FOR OPTICAL SIGNALING AND TACTILE SENSING

Abstract

Cephalopods such as octopuses have a combination of a stretchable skin and color-tuning organs to control both pressure and color for visual communications and disguise. We present an electroluminescent material that is capable of large uniaxial stretching and surface area changes while actively emitting light. Layers of transparent hydrogel electrodes sandwich a ZnS phosphor-doped dielectric elastomer layer, creating thin rubber sheets that change illuminance and capacitance under deformation. Arrays of individually controllable pixels in thin rubber sheets were fabricated using replica molding and were subjected to stretching, folding, and rolling to demonstrate their use as stretchable displays. These sheets were then integrated into the skin of a soft robot, providing it with dynamic coloration and sensory feedback from external and internal stimuli.

Introduction

Biological systems employ a host of strategies for visual display and camouflage. Cephalopods, for example, can mimic their environment by changing skin color and texture, as well as posture (1). Recent developments in soft robotics (2, 3), bioinspired design (4, 5), and stretchable electronics (6) reveal strategies that enable us to engineer some of the functions of cephalopod skin synthetically. For example, microfluidic networks filled with liquid dyes have been used as active camouflage and displays for soft mobile robots, giving them the ability to change their appearance via color, texture, and luminescence (7). More recently, electro-mechano-chemically responsive films were exploited to render fluorescent patterns under the control of electric fields (8), and adaptive optoelectronic camouflage systems have been used to mimic the visual appearance of cephalopod skin (9). Another approach is the use of active display technologies, such as polymeric light-emitting devices (PLEDs) and organic light-emitting diodes (OLEDs), which use stretchable transparent electrodes based on indium tin oxide (ITO) films (10), graphene (11), single- or multi-walled carbon

nanotubes (SWNTs or MWNTs) (12, 13), polyethylene-dioxythiophene: polystyrene-sulfonate (PEDOT: PSS) (14), or other percolated networks of conductive colloids or nanowires (15). Despite the broad applicability of LED-based systems for consumer displays, their electrical function is limited to ultimate strains, $\varepsilon_{ult} < 120\%$ (16), well below the ultimate strain of elastomers (such as silicones; ε_{ult} ~400 to 700%) that are used in soft robotics to mimic the movements of animals.

Biological skin also enables animals to sense their environments. A number of approaches have been used to create pressure-sensitive electronic skins, including arrays of organic field-effect transistors (FETs) deposited on flexible parylene-polyamide substrates (17, 18), and inside stretchable rubber (19), as well as thin Au films and liquid metal embedded in polydimethylsiloxane (PDMS) (20, 21). More recently, dielectric elastomer transducers (DETs), which are stretchable capacitors composed of highly extensible ionic hydrogels, have been used. These hydrogels are intrinsically soft, highly transparent in the visible spectrum (extinction coefficient $\mu_{ext} \sim 10^{-6}$ μm^{-1}) (22), can exhibit very high ultimate strain (ε_{ult}~2000%) and toughness ($U \sim 9$ kJ m^{-2}) (23), and

have relative changes in resistivity with strain that are orders of magnitude less than those of electrodes based on percolated networks of conductive particles (such as metal nanoparticles, carbon powder, or nanotubes) (24).

Presently, soft robots are primarily used because their low mechanical compliance enables safe human-robot interaction; however, their potential is limited by a lack of suitable electronics that can stretch continuously with their bodies. No soft robot can dynamically display information on its body, and there are relatively few examples that can sense external and internal stimuli. Here we present a hyperelastic light-emitting capacitor (HLEC) that enables both light emission and touch sensing in a thin rubber sheet that stretches to >480% strain (Fig. 1). These HLECs are composed of ionic hydrogel electrodes and composites of doped ZnS phosphors embedded in a dielectric matrix of silicone elastomer. We used electroluminescent (EL) phosphor powders that emit light via excitations within intrinsic heterojunctions under an AC electric field; unlike current-driven LEDs, which require lithography to form p-n junctions, this material system can be processed using replica molding. Application of an AC electric

field causes luminescence within the semiconducting phosphor at wavelength centers corresponding to the dopants in the ZnS lattice. Green and blue centers are typically produced using low [~0.01 weight % (wt %)] and high (~0.1 wt %) concentrations of Cu, whereas yellow is produced using Mn (~1 wt %) (25). White light can be achieved using combinations of these dopants.

Experimental Methods

The HLEC (**Fig. 2**) is a five-layer structure consisting of an electroluminescent dielectric layer that is sandwiched between two electrodes and encapsulated in low elastic modulus (E ~ 30 kPa) (***26***) silicone (Ecoflex 00-30, Smooth-on Inc.). Our hydrogel

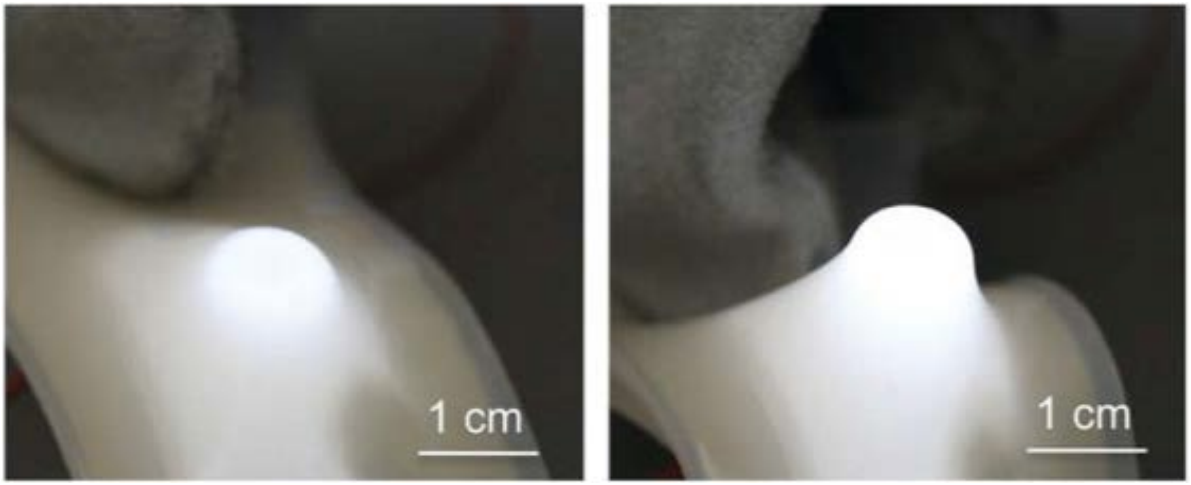

Figure 1. Image of the HLEC conforming to the end of a pencil

electrodes are designed with a balance of high mechanical toughness, low volatility, and low electrical resistance under deformation (Fig. S1). Aqueous lithium chloride (LiCl) is used as the ionic conductor because of its high conductivity (~10 S m^{-1}), ionic strength, and hygroscopic nature, whereas polyacrylamide (PAM) is used as the elastomeric matrix because of its high toughness (27) and optical transparency. Electrodes are synthesized by first dissolving acrylamide monomer (AAm), polyacrylamide (PAM), and *N*,*N*′-methylenebisacrylamide crosslinker (MBAA) in aqueous LiCl and casting the solution onto an ultraviolet (UV)–ozone–treated silicone (Ecoflex 00-30) substrate. The aqueous PAM-AAm solution is then crosslinked under UV light (28), producing a highly stretchable and transparent electrode. The EL layer is formed by mixing commercially available phosphor powders (Global Tungsten & Powders) (25 μm, ~8% by volume) into silicone (Ecoflex 00-30) and then molding the dispersion into a 1-mm-thick sheet. Finally, we bond the EL layer between the two electrode-patterned silicone substrates and encapsulate the capacitor in an insulating layer of silicone.

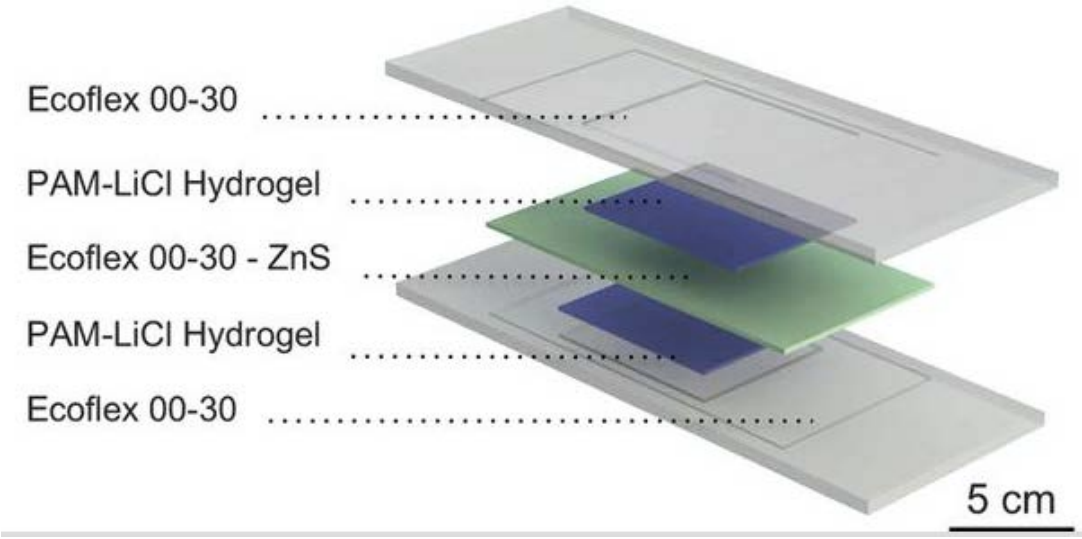

Figure 2. Exploded view of the HLEC showing its five-layer structure consisting of a ~1-mm-thick electroluminescent layer (ZnS-Ecoflex 00-30) that is sandwiched between two PAM-LiCl hydrogel electrodes and encapsulated in Ecoflex 00-30.

Results and Discussion

The stress-strain curves of the HLEC and its silicone-containing layers (Ecoflex and Ecoflex-EL composite) are all coincident, whereas the elastic modulus of the hydrogel is two orders of magnitude lower, allowing the HLEC to stretch freely without delaminating. Mechanical testing data (Fig. 3) and images (Fig. 4) show the excellent adhesion between the layers. The HLEC achieved a mean strain of 487 ± 59% (SD), as measured at five locations across the width of the illuminated section, with portions exceeding 500% before the external copper leads lost contact with the hydrogel electrodes.

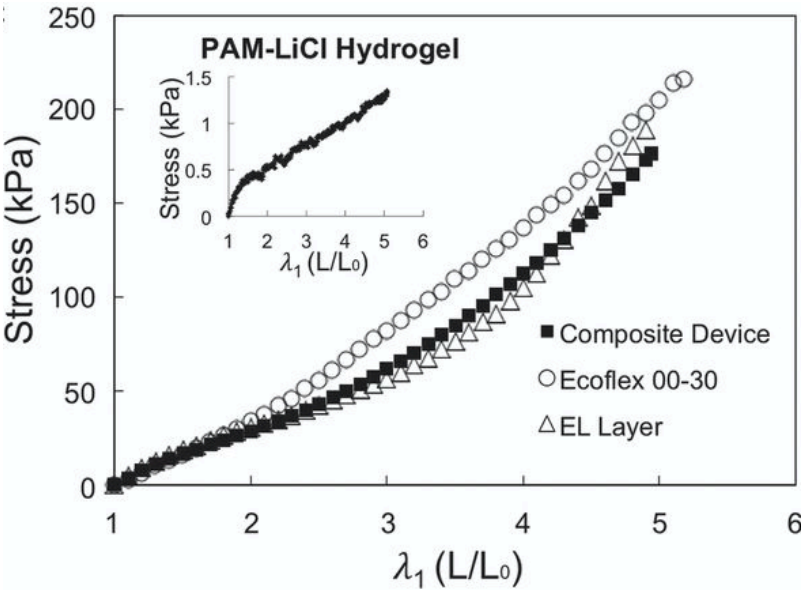

Figure 3. Stress-stretch curves of Ecoflex 00-30, the electroluminescent layer, and the composite device. The hydrogel data are shown in the inset because of its much lower elastic modulus.

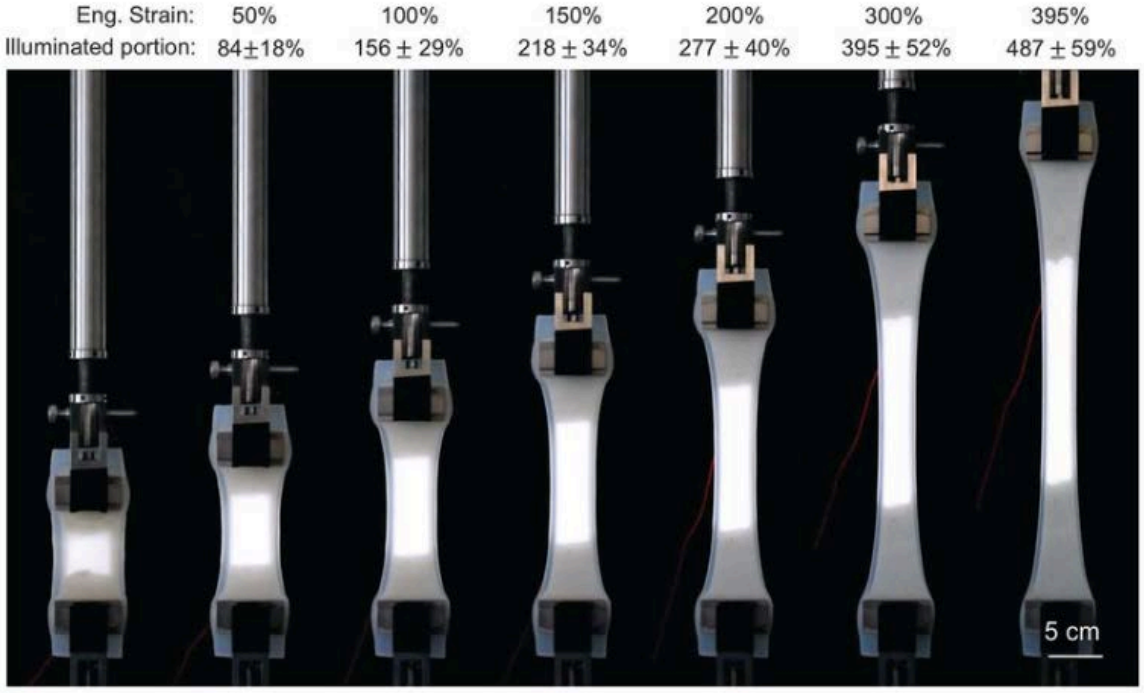

Figure 4. A nominal electric field of ~25 kV cm^{-1} was applied to the HLEC at the start of the uniaxial test. Five lengths were measured using image analysis software to obtain λ_1 across the width of the illuminated portion of the tensile bar. We report the mean and standard deviation of those measurements. At an engineering strain (grip to grip) of 395%, we measured the mean strain of the illuminated portion to be 487%, with a range of 420 to 549%.

For these tests, the HLECs were operated at 700 Hz under a nominal electric field of ~25 kV cm^{-1}, with a power consumption of 0.2 W and a luminous efficacy of 43.2 millilumens per watt (mlm W^{-1}) (28). We used this same replica molding technique to form an 8-by-8 array of 4-mm pixels (Fig. 5A). This HLEC display can undergo many deformation modes, including stretching, rolling, folding, and wrapping (Fig. 5, B to E). Dynamic control of the pixels is shown in Fig. 5, F to I).

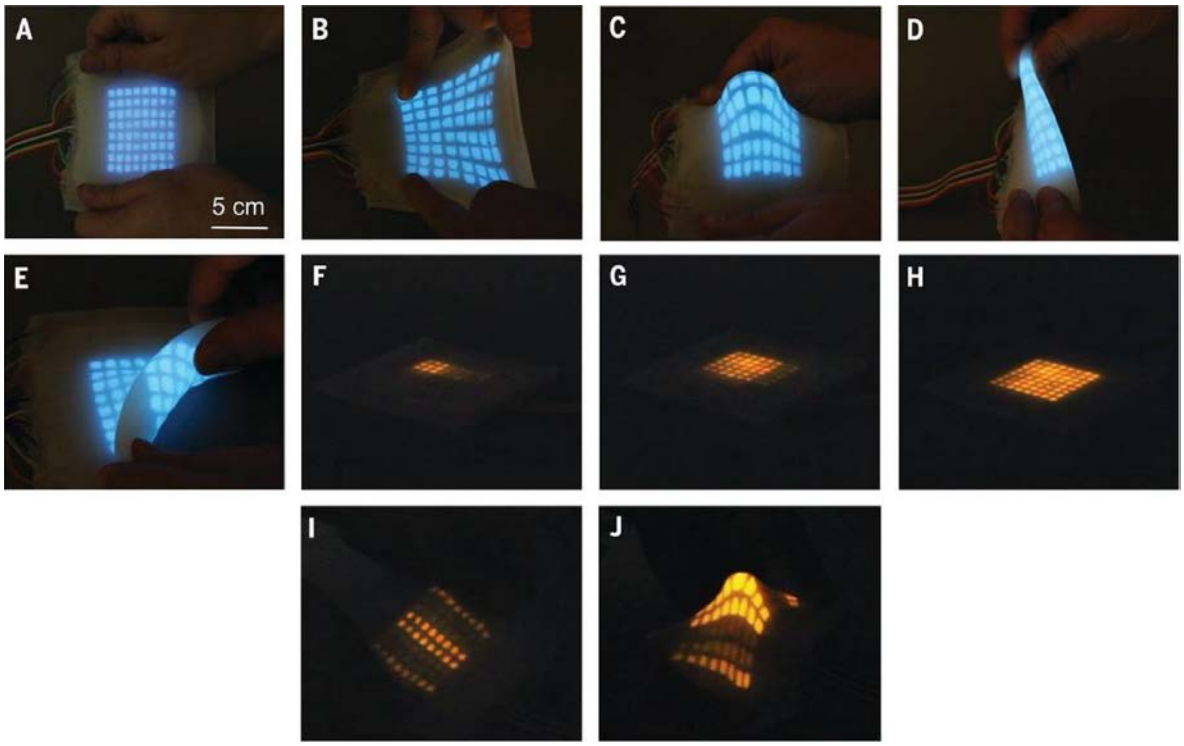

Figure 5. Multipixel electroluminescent displays fabricated via replica molding. The device measures 5 mm thick, with each of the 64 pixels measuring 4 mm. We show the devices in various states of deformation and illumination: (A) undeformed, (B) stretched, (C) wrapped around a finger, (D) folded, (E) rolled, (F to H) with subsets of pixels activated, and (I and J) subsets of pixels activated while being deformed.

In addition to emitting light, the HLEC also serves as a dielectric elastomer sensor (DES), due to its construction as a parallel-plate capacitor. Changes in the electrode area (A) and separation distance (d) cause the capacitance (C) to change according to $C/C_0 \propto Ad^{-1}$, allowing the HLEC to sense deformations from pressure and stretching. The capacitance of the HLEC changes as it is stretched under uniaxial (Fig. 6) and biaxial (Fig. S2) tension (28). We model the capacitance by expressing A and d in terms of the principal stretches, λ_1, λ_2, and λ_3, which represent the axial, transverse, and out-of-plane orientations, respectively (supplementary text). For uniaxial boundary conditions, we observe that the relative capacitance increases linearly as the sample is stretched (eq. S11). For biaxial test conditions, we observe that the relative change in capacitance follows $C/C_0 = \lambda^4$ (eq. S12); however, at higher strains, the measured values are slightly lower, due to a decrease in the permittivity of the dielectric (24).

The illuminance of the HLEC also increases as the device is stretched. We attribute this change to two interrelated phenomena: (i) the increase in electric field (E) as d decreases and (ii) the decrease in areal number density of phosphor particles (η)

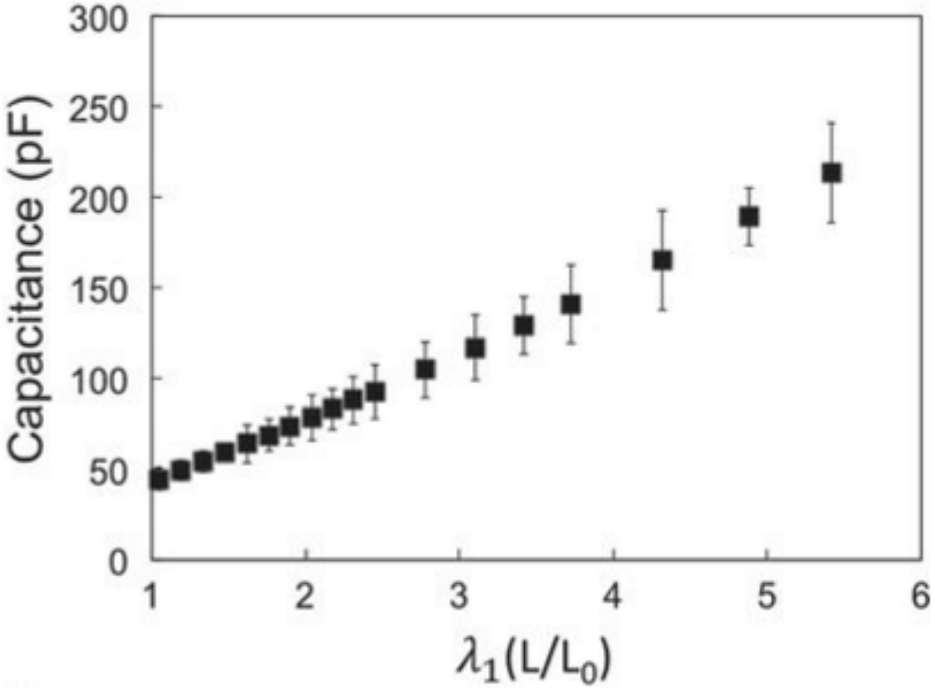

Figure 6. The capacitance of the HLEC as a function of its uniaxial stretch (number of samples, n = 4).

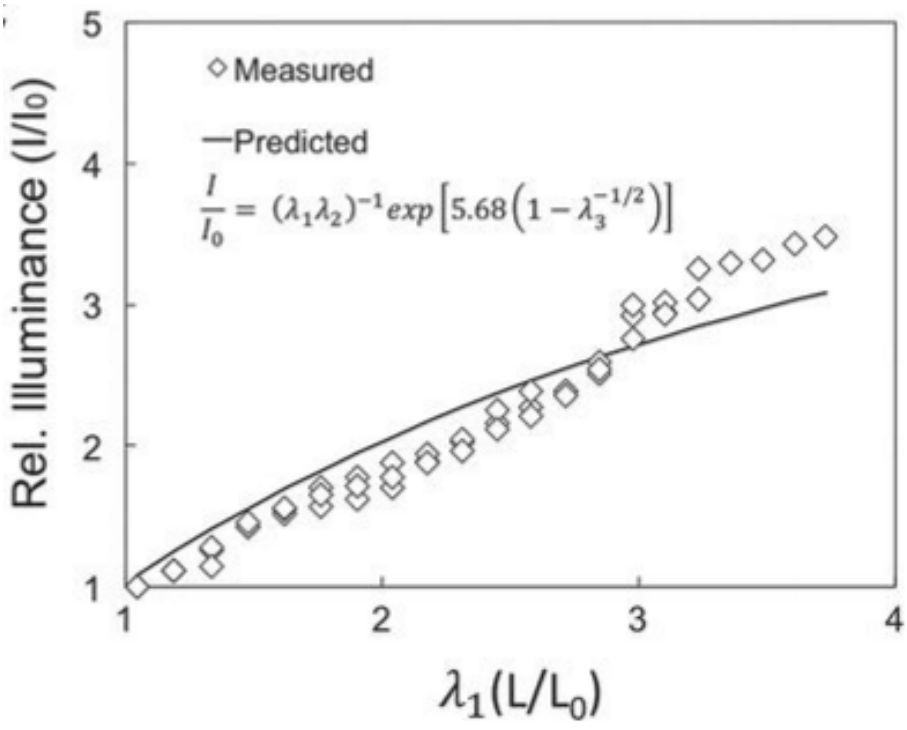

Figure 7. The relative illuminance of the HLEC versus its uniaxial stretch (n = 4), plotted alongside predicted values (supplementary text).

as A increases. Starting with the Alfrey-Taylor equation (eq. S13, Fig. S3) (29), we predict the scaling law in Eq. 1 by expressing E/E_0 as a function of the principal stretches and by correcting for the change in η with stretching ($\eta/\eta_0 \propto A_0/A$) (supplementary text). The predicted trend is shown alongside luminescence measurements in Fig. 7.

$$\frac{I}{I_0} = (\lambda_1\lambda_2)^{-1} exp[5.68(1-\lambda_3^{1/2}] \quad (1)$$

To demonstrate the ability to monolithically integrate the HLEC into soft systems, we embedded three HLEC panels in a crawling soft robot by bonding six layers together. The top four layers make up the electroluminescent skin, whereas the bottom two are used for pneumatic actuation (Fig. 8A). Inspired by architectures developed for mobile soft robots (30), our pneumatic actuator uses a series of inflatable chambers embedded in silicone, with a bottom layer composed of an inextensible fiber-elastomer composite (28). The inextensible layer induces a net bending moment as the pneumatic chambers are inflated; the resulting curvature is exploited to create an undulating gait.

The crawling robot uses its HLEC skin to sense its physical state and environment (i.e., proprioception and exteroception). The capacitance of the HLEC changes with

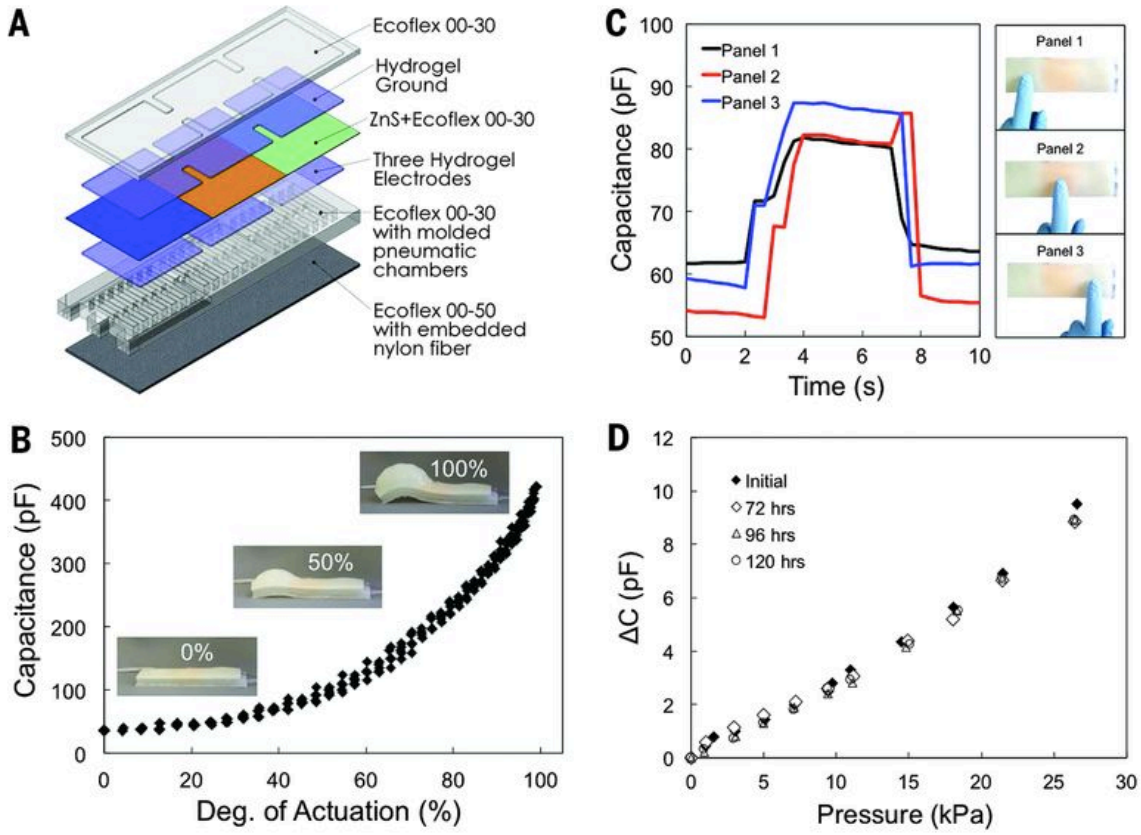

Figure 8. HLEC skins endow soft robots with the ability to sense their actuated state and environment and communicate optically. (A) Schematic of a three-chambered soft robot. A series of three independently actuated pneumatic chambers is embedded between the HLEC skin (top) and a strain-limiting layer (bottom). (B) Capacitance plotted versus the actuation amplitude, defined as the relative change in deflection between the uninflated and fully inflated states (number of samples, n = 5). (C) A firm finger press induces an ~25% increase in capacitance. (D) Change in capacitance versus applied pressure. We observed a negligible change in the capacitive response of the sensors over a period of 120 hours.

pneumatic actuation (Fig. 8B) and externally applied pressure (Fig. 8, C and D) (10).

Actuation of the three underlying pneumatic chambers results in capacitance changes (ΔC) of up to 1000% when the chambers are fully inflated. Additionally, each HLEC panel is largely decoupled from the state of the surrounding pneumatic chambers (Fig. S4) (28).

The ability to identify the actuated state of the robot using the capacitive sensor readings enables proprioception. To demonstrate the tactile sensing capabilities of the electronic skin, we pressed each of the HLEC panels on the robot and measured the capacitive response (Fig. 8C). A firm finger press resulted in a ~25% increase in capacitance. The relative capacitance versus applied pressure, ranging from 0.9 to 30.9 kPa, remained nearly constant over a period of 120 hours (Fig. 8D). Arrays of these tactile sensors enable exteroception in soft robotic systems.

An array of three HLEC panels patterned into the three-chambered crawling robot enables eight distinct illuminated states (Fig. 9A). The embedded HLEC remains functional as the robot is actuated through its crawling sequence (Fig. 9B). During actuation, the embedded HLEC undergoes stretches of $\lambda_1 = 2.63$ and $\lambda_2 = 2.42$ in the longitudinal (front to rear) and transverse (side to side) directions, respectively, to produce a ~635% increase in the skin's surface area (Fig. S5). Similar to the single-panel HLEC, the luminescence of the embedded skin increases during actuation as its thickness is decreased.

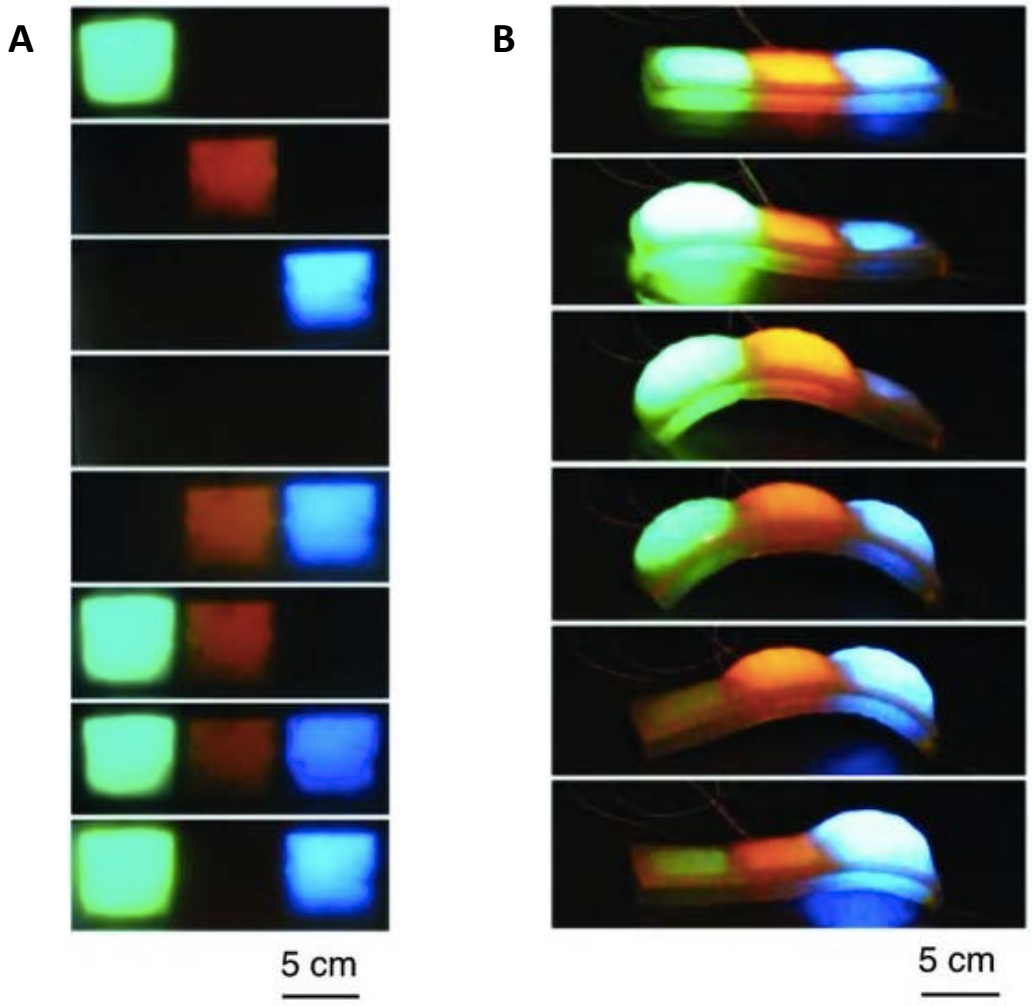

Figure 9. (A) Array of three HLEC panels, each emitting a different wavelength through selective doping of the EL phosphor layer. Each HLEC panel is activated independently. (B) An undulating gait is produced by pressurizing the chambers in sequence along the length of the crawler. This sequence produces forward locomotion at a speed of ~4.8 m hour^{-1} (~32 body lengths hour^{-1}). As each pneumatic chamber is pressurized, the outer electroluminescent skin is stretched, increasing the electric field across the EL layer and thus the luminescence.

Conclusion

Integrating these highly stretchable and compliant displays into soft actuators enables two new capabilities in soft electronics: (i) displays that actively change their

shape, and (ii) robots that actively change their color. Using replica molding, we fabricated a multipixel array of individually addressable HLECs, and we used the same process to monolithically integrate these displays into a soft robot capable of changing posture. The HLEC array imparts both dynamic coloration and the potential for feedback control, which would be useful in epidermal electronics (31) and robotics (32). Although the luminous efficacy of our HLEC (43.2 mlm W^{-1}) is not as high as that of commercial AC powder electroluminescent devices (~4 lm W^{-1}) (33), it can be greatly improved by tuning the materials system and device architecture (such as higher-transmissivity encapsulation layers, reduced thickness, and optimized particle size). For applications requiring higher display resolution, HLECs could be made compatible with photolithography and other microfabrication techniques by using photopolymerizable polymers. These techniques would also allow us to decrease the thickness of the electroluminescent layer, thereby reducing the voltage required to power the HLEC.

REFERENCE

1. A. Barbosa, J. J. Allen, L. Mäthger, R. T. Hanlon, Cuttlefish use visual cues to determine arm postures for camouflage. *Proc. R. Soc. London Ser. B.* **279**, 84-90 (2012).
2. F. Ilievski, A. D. Mazzeo, R. F. Shepherd, X. Chen, G. M. Whitesides, Soft robotics for chemists. *Angew. Chem. Int. Ed. Engl.* **50**, 1890-1895 (2011).
3. D. Rus, M. T. Tolley, Design, fabrication and control of soft robots. *Nature* **521**, 467-475 (2015).
4. M. J. Spenko, G. C. Haynes, J. A. Sanders, M. R. Cutkosky, A. A. Rizzi, Biologically inspired climbing with a hexapedal robot. *J. Field Robot.* **25**, 223-242 (2008).
5. E. Kreit, L. M. Mäthger, R. T. Hanlon, P. B. Dennis, R. R. Naik, E. Forsythe, J. Heikenfeld, Biological versus electronic adaptive coloration: How can on inform the other? *J. R. Soc. Interface* **10**, 20120601 (2012).
6. J. A. Rogers, T. Someya, Y. Huang, Materials and mechanics for stretchable electronics. *Science* **327**, 1603-1607 (2010).
7. S. A. Morin, R. F. Shepherd, S. W. Kwok, A. A. Stokes, A. Nemiroski, G. M. Whitesides, Camouflage and display for soft machines. *Science* **337**, 828-832 (2012).

8. Q. Wang, G. R. Gossweiler, S. L. Craig, X. Zhao, Cephalopod-inspired design of electro-mechano-chemically responsive elastomers for on-demand fluorescent patterning. *Nat. Commun.* **5**, 4899 (2014).
9. C. Yu, Y. Li, X. Zhang, V. Malyarchuk, S. Wang, Y. Shi, L. Gao, Y. Su, Y. Zhang, H. Xu, R. T. Hanon, Y. Huang, J. A. Rogers, Adaptive optoelectronic camouflage systems with designs inspired by cephalopod skins. *Proc. Natl. Acad. Sci. U.S.A.* **111**, 12998-13003 (2014).
10. P. E. Burrows, G. L. Graff, M. E. Gross, P. M. Martin, M. K. Shi, M. Hall, E. Mast, C. Bonham, W. Bennett, M. B. Sullivan, Ultra barrier flexible substrates for flat panel displays. *Displays* **22**, 65-69 (2001).
11. T. H. Han, Y. Lee, M.-R. Choi, S.-H. Woo, S.-H. Bae, B. H. Hong, J.-H. Ahn, T.-W. Lee, Extremely efficient flexible organic light-emitting diodes with modified graphene anode. *Nat. Photonics* **6**, 105-110 (2012).
12. T. Sekitani, H. Nakajima, H. Maeda, T. Fukushima, T. Aida, K. Hata, T. Someya, Stretchable active-matrix organic light-emitting diode display using printable elastic conductors. *Nat. Mater.* **8**, 494-499 (2009).
13. M. K. Shin, J. Oh, M. Lima, M. E. Kozlov, S. J. Kim, R. H. Baughman, Elastomeric conductive composites based on carbon nanotube forests. *Adv. Mater.* **22**, 2663-2667 (2010).

14. M. S. White, M. Kaltenbrunner, E. D. Gtowacki, K. Gutnichenko, G. Kettlgruber, I. Graz, S. Aazou, C. Ulbricht, D. A. M. Egbe, M. C. Miron, Z. Major, M. C. Scharber, T. Sekitani, T. Someya, S. Bauer, N. S. Sariciftci, Ultrathin, highly flexible and stretchable PLEDs. *Nat. Photonics.* **7**, 811-816 (2013).

15. L. Hu, H. S. Kim, J. Y. Lee, P. Peumans, Y. Cui, Scalable coating and properties of transparent, flexible, silver nanowire electrodes. *ACS Nano* **4**, 2955-2963 (2010).

16. J. Liang, L. Li, X. Niu, Z. Yu, Q. Pei, Elastomeric polymer light-emitting devices and displays. *Nat. Photonics* **7**, 817-824 (2013).

17. T. Someya, Y. Kato, T. Sekitani, S. Iba, Y. Noguchi, Y. Murase, H. Kawaguchi, T. Sakurai, Conformable, flexible, large-area networks of pressure and thermal sensors with organic transistor active matrixes. *Proc. Natl. Acad. Sci. U.S.A.* **102**, 12321-12325 (2005).

18. K. Takei, T. Takahashi, J. C. Ho, H. Ko, A. G. Gillies, P. W. Leu, R. S. Fearing, A. Javey, Nanowire active-matrix circuitry for low-voltage macroscale artificial skin. *Nat. Mater.* **9**, 821-826 (2010).

19. T. Someya, T. Sekitani, S. Iba, Y. Kato, H. Kawaguchi, T. Sakurai, A large-area, flexible pressure sensor matrix with organic field-effect transistors for artificial skin applications. *Proc. Natl. Acad. Sci. U.S.A.* **101**, 9966-9970 (2004).

20. Y. L. Park, B. R. Chen, R. J. Wood, Design and fabrication of soft artificial skin using embedded microchannels and liquid conductors. *IEEE Sens. J.* **12**, 2711-2718 (2012).

21. D. P. J. Cotton, I. M. Graz, S. P. Lacour, A multifunctional capacitive sensor for stretchable electronic skins. *IEEE Sens. J.* **9**, 2008-2009 (2009).

22. C. Keplinger, J. Y. Sun, C. C. Foo, P. Rothemund, G. M. Whitesides, Z. Suo, Stretchable, transparent, ionic conductors. *Science* **341**, 984-987 (2013).

23. J. Y. Sun, X. Zhao, W. R. Illeperuma, O. Chaudhuri, K. H. Oh, D. J. Mooney, J. J. Vlassak, Z. Suo, Highly stretchable and touch hydrogels, *Nature* **489**, 133-136 (2012).

24. J. Y. Sun, C. Keplinger, G. M. Whitesides, Z. Suo, Ionic skin. *Adv. Mater.* **26**, 7608-7614 (2014).

25. A. Kitai, *Luminescent Materials and Applications* (Wiley, West Sussex, UK, 2008), pp. 249-268.

26. R. F. Shepherd, A. A. Stokes, R. M. D. Nunes, G. M. Whitesides, Soft machines that are resistant to puncture and that self seal. *Adv. Mater.* **25**, 6709-6713 (2013).

27. Y. Bai, B. Chen, F. Xiang, J. Zhou, H. Wang, Z. Suo, Transparent hydrogel with enhanced water retention capacity by introducing highly hydratable salt. *Appl. Phys. Lett.* **105**, 151903 (2014).

28. Materials and methods are available in Chapter 2: Supplementary Materials.

29. G. F. Alfrey, J. B. Taylor, Electroluminescence in single crystals of zinc sulphide. *Proc. Phys. Soc. B* **68**, 775 (1955).

30. R. F. Shepherd, F. Ilievski, W. Choi, S. A. Morin, A. A. Stokes, A. D. Mazzeo, X. Chen, M. Wang, G. M. Whitesides, Multigait soft robot. *Proc. Natl. Acad. Sci. U.S.A.* **108**, 20400-20403 (2011).

31. D. H. Kim, N. Lu, R. Ma, Y. S. Kim, R. H. Kim, S. Wang, J. Wu, S. M. Won, H. Tao, A. Islam, K. J. Yu, T. I. Kim, R. Chowdhury, M. Ying, L. Xu, M. Li, H. J. Chung, H. Keum, M. McCormick, P. Liu, Y. W. Zhang, F. G. Omenetto, Y. Huang, T. Coleman, J. A. Rogers, Epidermal Electronics, *Science* **333**, 838-843 (2011).

32. J. Kim, M. Lee, H. J. Shim, R. Ghaffari, H. R. Cho, D. Son, Y. H. Jung, M. Soh, C. Choi, S. Jung, K. Chu, D. Jeon, S. T. Lee, J. H. Kim, S. H. Choi, T. Hyeon, D. H. Kim, Stretchable silicon nanoribbon electronics for skin prosthesis. *Nat. Commun.* **5**, 5747 (2014).

33. A. T. Conn, J. Rossiter, Smart radially folding structures. *Mechatronics IEEE/ASME Trans.* **17**, 968-975 (2012).

CHAPTER 3

SUPPLEMENTARY MATERIALS FOR HIGHLY STRETCHABLE ELECTROLUMIENSCENT SKIN FOR OPTICAL SIGNALING AND TACTILE SENSING

Materials and Methods

Materials

The hyperelastic light emitting capacitor (HLEC) and crawling robot are composed of intrinsically soft materials: silicones (Ecoflex 00-30; Smooth-On Inc.), polyacrylamide based LiCl hydrogel electrodes, and transition metal-doped ZnS phosphors (Global Tungsten & Powders Corp.) embedded in Ecoflex 00-30 as the active display material. Hydrogels are synthesized using acrylamide (AAm; Sigma-Aldrich) and polyacrylamide (PAM, Mw ~$5x10^6$) (92560; Sigma-Aldrich) swelled in aqueous LiCl (LiCl; Alfa Aesar) along with a crosslinker (N, N'-methylenebisacrylamide, or MBAA; Sigma-Aldrich) and a photoinitiator (Irgacure 1173; BASF). AAm and LiCl are dissolved in deionized water at a concentration of 1.75 M and 8 M, respectively, followed by PAM at a weight ratio of 0.142 PAM:AAm. The solution is mixed on a magnetic stirrer at 60 °C for 4 hours, and then MBAA and Irgacure 1173 are added at a weight ratio of 0.01 and 0.016:

AAm, respectively. Mixing for two additional hours yields the uncured hydrogel electrode material.

Hyperelastic Light-Emitting Capacitor (HLEC) fabrication

The synthetic skin is fabricated using replica molding. The outer layers (see Fig. 2) are formed by casting Ecoflex 00-30 into 3D printed molds (Objet 30; Stratasys Ltd.) followed by curing at 80 °C for 20 minutes. We treated the bonding surfaces with UV-ozone for 10 minutes. We poured the uncured hydrogel into the 1 mm electrode relief pattern and cured it for 15 seconds under UV light (320-500 nm, 200 W) (Model S1500; Lumen Dynamics) to create the top and bottom electrodes. We formed the electroluminescent (EL) layer by mixing EL phosphor powders with Ecoflex 00-30 (7.8 wt. % phosphor), and then casting the dispersion into the 1 mm relief pattern (cured at ~80°C). We use orange (GGL11X), green (GG41X), blue (GGL61X), and white (GGL71X) phosphor powders (Global Tungsten and Powder Corp.) to produce the colors shown in this manuscript. The entire structure is encapsulated in Ecoflex 00-30. The resulting device has a total thickness of 8 mm with staggered electrodes that enable

connection to an external power source using stranded copper wire inserted through the silicone.

Integration of HLEC into a crawling soft robot

HLECs are molded into the body of the soft robotic crawler as shown in (Fig. 8A, Fig. S6). Plastic molds were 3D printed for each layer (Objet 30; Stratasys Ltd.). Three independently controlled inflatable chambers actuate the front, middle, and rear sections of the robot. The extensible top layer of the robot contains separate reservoirs for each of the three electrodes, while the bottom is bonded to an inextensible elastomeric composite consisting of a woven nylon sheet (9318T18, McMaster-Carr Supply Co.) embedded in silicone (Ecoflex 00-50; Smooth-On Inc.). The top electrodes and encapsulation layers are then added using general HLEC fabrication methods.

Capacitance and luminescence of HLEC vs. stretching

Capacitance was measured under uniaxial stretch by connecting a capacitance meter (830C; BK Precision) to the hydrogel electrodes using stranded copper wires. Luminescence of the HLEC was observed and measured under uniaxial stretching using a

mechanical tester (Z010; Zwick Roell) and a portable light meter (HHLM 1337; Omega Engineering Inc.). Specimens were mounted on the machine, connected to an alternating current (AC) voltage source (2.5 kV, 700 Hz), and subjected to uniaxial tension. We used a high-voltage amplifier (610D; TREK Inc.) coupled with a function generator (3312 A; Hewlett Packard) to power the HLEC. A strain rate of 100% min-1 was used in all tests. The engineering strain (grip-to-grip) was recorded using the controller software, while the strain within the luminescent area was measured from recorded video using Image-J. The illuminance was measured by placing the light meter ~5 mm from the center of the luminescent area with a shield to block interference from ambient light.

Biaxial stretching of HLEC

Biaxial stretching was performed using a radially folding acrylic frame (Fig. S2B, C) (33). Circular test specimens (50 mm diameter) were fabricated using replica molding with 3D printed molds (UP Plus 2; Beijing TierTime Technology Co. Ltd). Each test specimen contained a 20 mm HLEC. The test samples were bonded to the frame (SilPoxy; Smooth-On Inc.) and their capacitance was measured (830C; BK Precision) at set intervals

as the frame was expanded. The collected data is plotted in (Fig. 4).

Exteroception and proprioception of electroluminescent skin

Capacitance measurements were taken on the electroluminescent skin embedded in the soft robot. The top and bottom hydrogel electrodes were connected to the capacitance meter. A program written in Processing was used to communicate with the capacitance meter and an ATmega328 microcontroller (Arduino Uno R3; Adafruit). This program coordinates data retrieval and logging from the capacitance meter and controls a solenoid valve to pressurize each chamber. The solenoid valve is activated using a signal from the ATmega328 to precisely time the input of pressurized air into the actuator. The testing apparatus is shown in Fig. S4B. Pressure from human touch was measured on individual panels. The applied force was manually controlled by simply pressing each panel. Capacitance measurements were also taken on the panel as known weights were applied externally to the panel and as the underlying pneumatic chambers were pressurized (compressed air, 7 psi, ~48 kPa). The degree of actuation was defined based on the morphology of the undulation, which we control using input pressure and time. Lastly, we

measured the capacitance (Fig. S4C) of the center pneumatic chamber in each possible state of the surrounding chambers (Fig. S4A).

Soft robot locomotion

The undulating gait used for crawling included six steps: (i) only the rear chamber pressurized, (ii) rear and middle chambers pressurized, (iii) all three chambers pressurized, (iv) middle and front chambers pressurized, (v) front chamber pressurized, and (vi) no chambers pressurized. Each actuation was driven by a nominal pressure of 4.7 psi (~32 kPa). This sequence produces forward locomotion at a speed of ~4.8 m hr^{-1} (~32 body lengths hr^{-1}). Panel illumination during crawling was powered by an amplifier (610D; TREK Inc.).

Resistance of hydrogel electrode under uniaxial strain

The resistance of hydrogel was examined under uniaxial strain using a precision LCR meter (E4980A; Agilent). All measurements were conducted with a 5 mm gage length. The nominal (or unstretched) resistance was 59.96 ± 1.93 Ω (SD), while at 300% strain it increased to 144.33 ± 4.99 Ω (SD). We also examined the cyclic resistance

variation of the electrodes by measuring resistance over 10 successive stretching cycles; we observed negligible resistance variation (Fig. S1).

Illuminance of HLEC as a function of voltage

The illuminance (luminous flux per unit area, measured in lux) of the HLEC was measured using a light meter (HHLM 1337; Omega Engineering Inc.). Samples were pre-stretched ($\varepsilon = 135\%$), mounted on the tensile tester (Z010; Zwick Roell), and connected to the external voltage source. Illuminance was measured as a function of voltage (at 700 Hz). The light meter was held at a distance of 5 mm from the center of the HLEC in all tests. As shown in Figure S3, the illuminance increases by a factor of ~20 as the voltage is increased from 2.5 - 5 kV (in accordance with Eq. S13).

Power consumption and luminous efficacy

We used a simple test circuit (Fig. S7) to measure the power consumption of the HLEC (Fig. 4) while illuminated in its unstretched state. We applied an AC waveform using a high-voltage amplifier (610D; TREK Inc.) coupled with a function generator (3312 A; Hewlett Packard). We applied a nominal voltage input of 2.5 kV at 700 Hz to the high

voltage input of the test circuit. We used a multimeter (83V; Fluke Corp.) to 7 measure $V_{RMS,\,BA}$ (the root mean square, RMS, voltage across R_2), $V_{RMS,A}$ (the RMS voltage across R_1), and the resistance of each resistor (Table S1). We calculated the RMS current across each resistor using $IRMS = V_{RMS}R^{-1}$. Using Kirchhoff's current law, we equated the current through resistors 1 and 2:

$$I_{RMS,2} = \frac{V_{RMS,BA}}{R_2} = \frac{V_{RMS,A}}{R_3} = I_{RMS,3} \quad \text{(S1)}$$

Using Eq. S1, we calculated $V_{RMS,\,CA}$ (the voltage across the entire test circuit):

$$V_{RMS,CA} = V_{RMS,CB} + V_{RMS,BA} = (1 + \frac{R_3}{R_2})V_{RMS,BA} \quad \text{(S2)}$$

The current across the first resistor (R_1) is equal to the total current through the test circuit. Using this equality, we calculated the power of the test circuit using

$$P_{real,total} = I_{RMS,total}\, V_{RMS,total} cos\theta = I_{RMS,1} V_{RMS,CA} cos\theta \quad \text{(S3)}$$

where θ represents the phase shift between the current and voltage waveforms across the test circuit. This phase shift was measured using an oscilloscope (TDS 1012; Tektronix) (Table S1). We calculated the real power of the test circuit to be 1.86 W. This power consumption includes energy used by the HLEC and the resistors according to

$$P_{total} = P_{HLEC} + P_{resistors} \quad \text{(S4)}$$

We subtracted the power consumption of the resistors to find the power consumption of the HLEC. We used $P=V_{RMS}I_{RMS}$ to calculate the power consumed by each resistor. The cumulative power consumption of the three resistors was 1.66 W. Therefore the power consumption of the illuminated HLEC (Fig. 4) was approximately 0.20 W. The illuminance of this HLEC was measured to be 4.32 cd sr m^{-2} (Model HHLM 1337; Omega Engineering Inc.), with a calculated luminous efficacy of 43.2 millilumens per Watt (mlm W^{-1}).

Mechanical testing

Stress-strain curves were measured for Ecoflex 00-30 (Smooth-On Inc) with and without embedded ZnS phosphor powders (25μm), PAM-LiCl hydrogel and the composite HLEC using a tensile tester (Z010; Zwick Roell). A strain rate of 100% min^{-1} was used in all tests. The engineering strain (grip-to-grip) was recorded using the controller software, while the strain within the luminescent area was measured from recorded video using Image-J.

Supplementary Text

Capacitance v. strain

The capacitance of a parallel plate capacitor in the stretched (C) and unstretched (C_0) states scales according to Eq. S5 and Eq. S6, respectively. We use this basic model to understand how the capacitance of the HLEC behaves as the area (A) and thickness (d) are changed.

$$C \propto \frac{A}{d} \tag{S5}$$

$$C_0 \propto \frac{A_0}{d_0} \tag{S6}$$

For uniaxial stretching, we approximate the relative change in the electrode area (A) and separation distance (d) using Eq. S7 and Eq. S8, respectively. Here, λ_1, λ_2, and λ_3 represent the axial, transverse, and out-of-plane stretches of the illuminated portion of the HLEC. Still-frames extracted from video taken of the uniaxial tension test were measured in Image-J to determine λ_1 and λ_2, and then the condition of incompressibility (Eq. S9) was invoked to determine λ_3.

$$A = A_0\lambda_1\lambda_2 \tag{S7}$$

$$d = d_0\lambda_3 \tag{S8}$$

$$\lambda_1\lambda_2\lambda_3 = 1 \tag{S9}$$

Combining Equations S5-S9 yields the scaling law for the capacitance of the HLEC (Eq. S10).

$$\frac{C}{C_0} = \lambda_1^2\lambda_2^2 \tag{S10}$$

For an incompressible material (Eq. S9) under uniaxial tension, we expect $\lambda_2 = \lambda_3 = \lambda_1^{-1/2}$ as the sample is stretched axially (along λ_1). Applying this boundary condition to Eq. S10, we expect that the relative capacitance under uniaxial tension scales according to

$$\frac{C}{C_0} = \lambda_1 \tag{S11}$$

For an incompressible material (Eq. S9) under biaxial tension, we impose $\lambda_1 = \lambda_2$. Applying this boundary condition to Eq. S10, we expect that the relative capacitance under biaxial tension scales according to

$$\frac{C}{C_0} = \lambda_1^4 \tag{S12}$$

Intensity vs. voltage and strain

Here we use the Alfrey-Taylor model (29) to predict how the illuminance changes as a function of stretching in uniaxial tension. We start with Equation S13, which expresses the relative illuminance (I/I_0) as a function of applied voltage (V). From Figure S3, we observe that the HLEC behaves in accordance with Eq. S13. The fitting parameter (b = 15.71) was calculated using a least squares fit ($R^2 = 0.983$).

$$\frac{I}{I_0} = \exp[b(V_0^{-1/2} - V^{1/2})] \quad \text{(S13)}$$

Our goal is to express Eq. S13 in terms of the principal stretches along the axial, transverse, and out-of-plane directions in our uniaxial tension test (λ_1, λ_2, and λ_3, respectively). First we replace the voltage terms with electric field, E, using the relation $E = Vd^{-1}$ to yield Eq. S14.

$$\frac{I}{I_0} = \exp[b(E_0 d_0)^{-\frac{1}{2}} - (Ed)^{-\frac{1}{2}}] \quad \text{(S14)}$$

where E_0 represents the nominal electric field (~2.5 kV cm^{-1}). We then invoke Eq. S8 to obtain

$$\frac{I}{I_0} = \exp[a(1 - \lambda_3^{1/2})] \quad \text{(S15)}$$

where $a = b(E_0 - d_0)^{-1/2}$. We also must account for the change in areal number density of EL particles, η, as the electrode area, A, increases. We propose that this affects the illuminance inversely according to the following scaling law:

$$\frac{I}{I_0} \propto \frac{\eta}{\eta_0} \propto \frac{A_0}{A} \tag{S16}$$

Combining Equations S7, S15, and S16 yields the relative change in intensity as a function of physical parameters that can be measured in the uniaxial tension test (λ_1, λ_2, and λ_3):

$$\frac{I}{I_0} = (\lambda_1\lambda_2)^{-1}\exp[a(1-\lambda_3^{1/2})] \tag{S17}$$

The illuminance was measured in uniaxial tension using a portable light meter (Model HHLM 1337; Omega Engineering Inc.). The results are shown in Fig. 2C, along values predicted using Eq. S17. The fitting parameter (a = 5.68) was calculated using a least squares fit (R^2 = 0.902).

Supplementary Figures

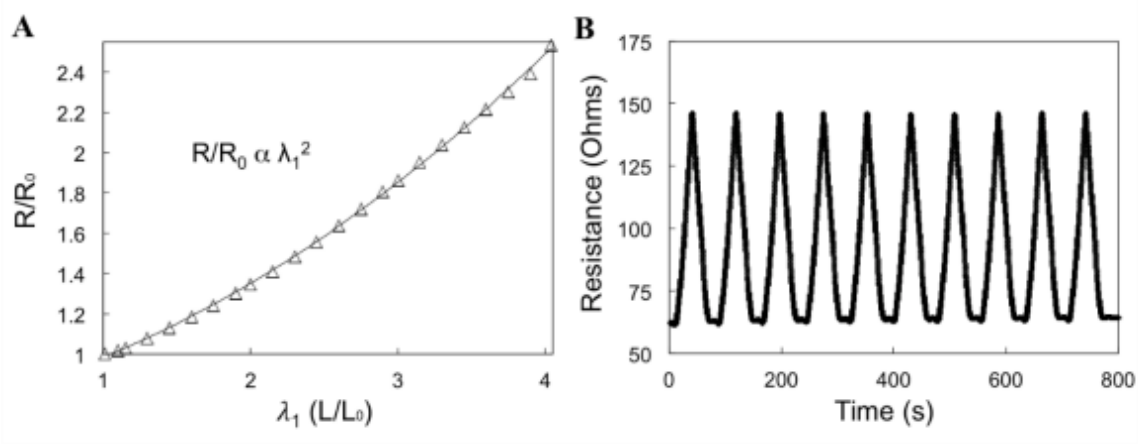

Figure S1. Resistive behavior of PAM-LiCl hydrogel. (A) The relative change in hydrogel resistance (R/R_0) increases with uniaxial strain (n = 5; standard deviation within markers). The relative change in resistance scales with λ^2 (note: $\lambda = \varepsilon + 1$), and is consistent with recently reported conductive acrylamide hydrogel chemistries (22, 24). (B) The hydrogel under cyclic loading for 10 cycles.

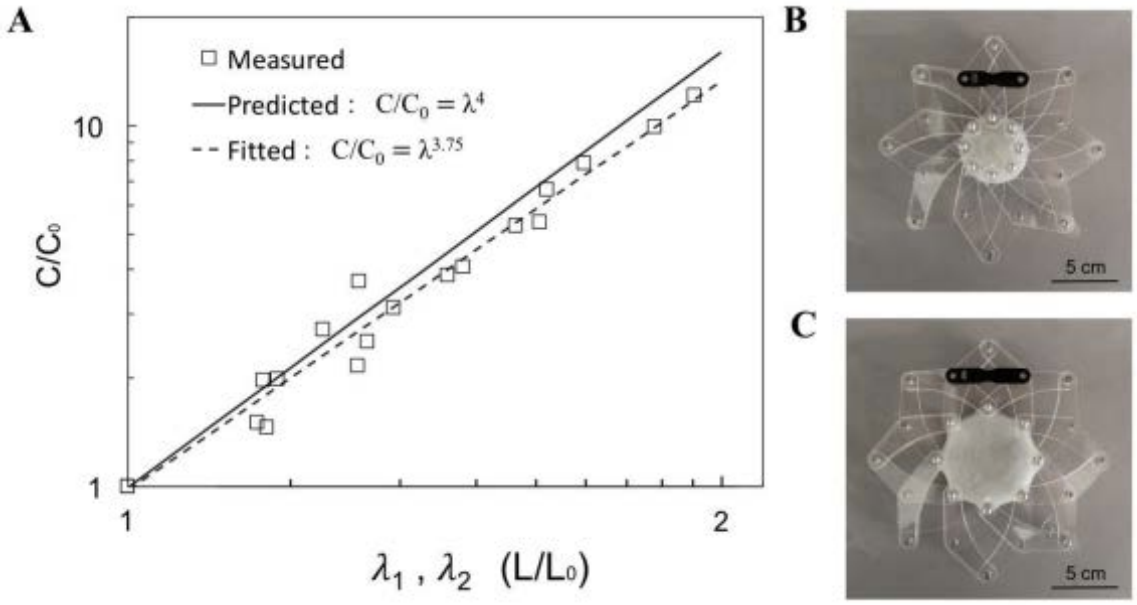

Figure S2. Capacitance of the HLEC in equibiaxial tension. (A) The relative change in capacitance follows the λ^4 dependence predicted in Eq. S12 (n = 3). (B) A circular HLEC test sample mounted in the biaxial test apparatus in the unstretched state. (C) The HLEC sample being stretched biaxially, with intervals set by a series of black acrylic linkages.

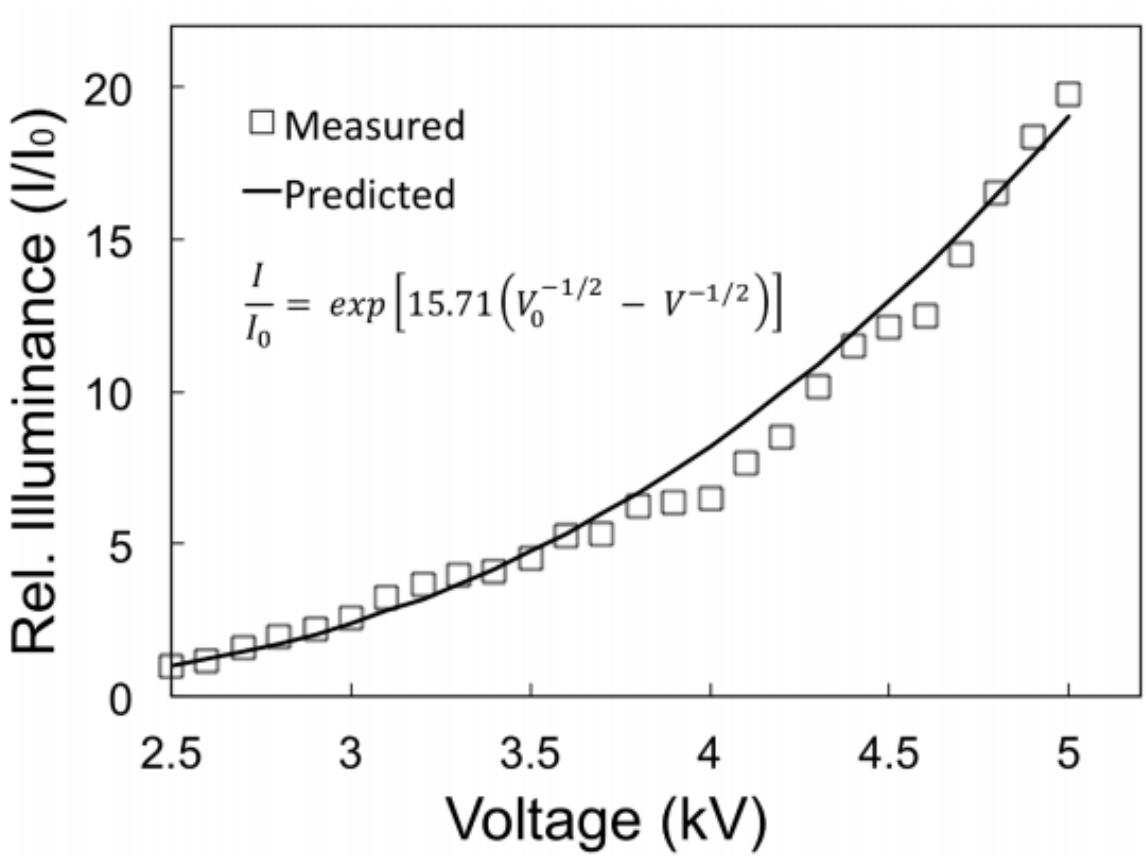

Figure S3. Relative illuminance of the HLEC versus voltage. Measurements are taken in the prestretched state (ε = 135%) at a constant frequency (700 Hz). Predicted values are calculated using Eq. S13. The fitting parameter (b = 15.71) was calculated using a least squares fit (R^2 = 0.983).

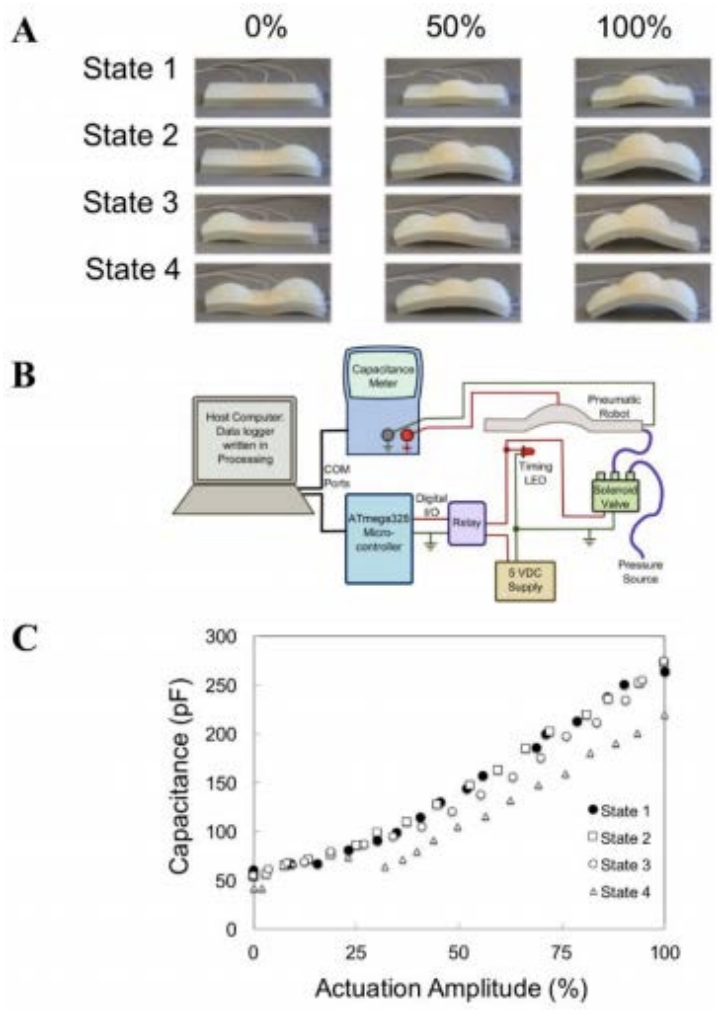

Figure S4. Capacitance of the center HLEC panel measured as a function of actuation amplitude for various system states. (A) The system states are shown visually; *State 1*: left and right panels non-pressurized, *State 2*: left panel non-pressurized, right panel pressurized, *State 3*: left panel pressurized, right panel non-pressurized, and *State 4*: left and right panels pressurized. (B) Experimental setup for measuring capacitance as pneumatic chambers are inflated. (C) Capacitance of the center HLEC as a function of the actuation amplitude of the center pneumatic chamber for each of the four states. The capacitance is largely independent of the actuation level of neighboring chambers.

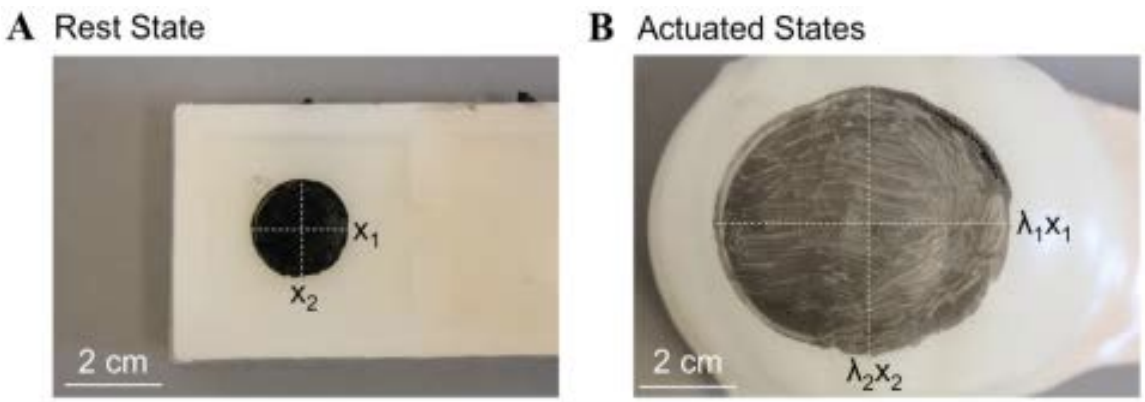

Figure S5. Deformation of the HLEC during pneumatic actuation of the robot. The principal stretches, λ_1 and λ_2, which correspond to the longitudinal (x_1) and transverse (x_2) directions, respectively, were measured as the robot was actuated through the crawling sequence (shown in Fig. 9B). (A) A circular fiducial mark was placed on the HLEC and measured along its major (x_1) and minor (x_2) axes. (B) The principal stretches shown in this figure are $\lambda_1 = 2.63$ and $\lambda_2 = 2.42$. These measurements account for out-of-plane deformation of the inflated chamber (not captured in this 2D image). We observe that the surface area of the ellipse in the deformed state is ~635% larger than the nominal circular fiducial mark in the rest state ($A/A_0 = \lambda_1 \lambda_2$).

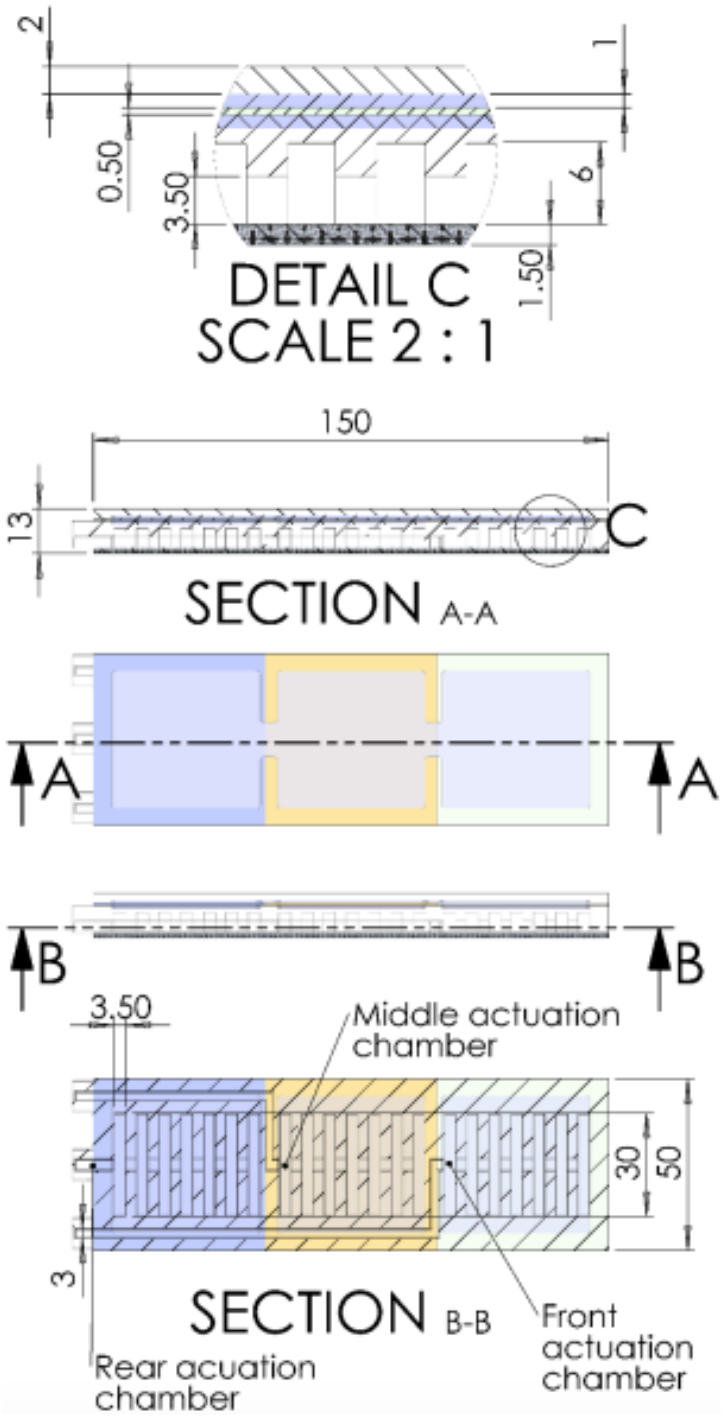

Figure S6. Dimensioned drawing of the soft robot. The robot has three independently actuated pneumatic chambers corresponding to three HLEC panels. Dimensions are shown in mm.

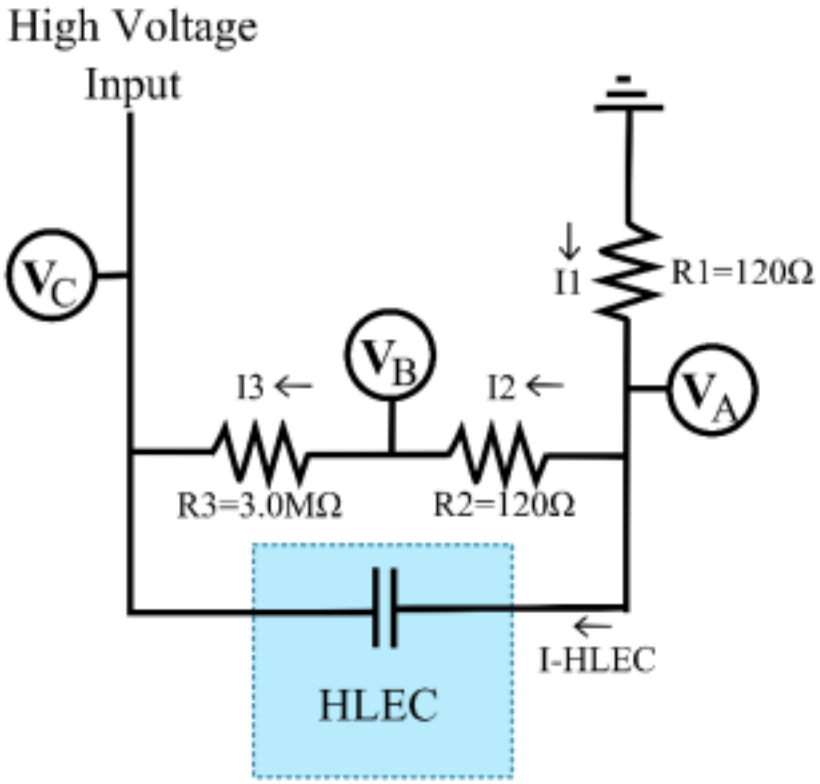

Figure S7. Test circuit used to measure power consumption of the HLEC.

Supplementary Table

Table S1. Power consumption measurements for the HLEC. The test circuit used to measure these values is shown in Fig. S7.

$V_{RMS,BA}$ (mV)	88.2
$V_{RMS,A}$ (mV)	101.5
R_1 (Ω)	118.3
R_2 (Ω)	118.6
R_3 (MΩ)	2.993
θ (°)	13.5